PROBABILISTIC MODELS FOR DAMAGE AND REPAIR COST FOR REINFORCED CONCRETE STRUCTURAL MEMBERS

by

Shahrzad Talachian

B.A., American University of Sharjah, 2007

A THESIS SUBMITTED IN PARTIAL FULFILLMENT OF
THE REQUIREMENTS FOR THE DEGREE OF

MASTER OF APPLIED SCIENCE

in

The Faculty of Graduate Studies

(Civil Engineering)

THE UNIVERSITY OF BRITISH COLUMBIA
(Vancouver)

DECEMBER 2010

© Shahrzad Talachian, 2010

Abstract

The context of this thesis is performance-based engineering, in which the prediction of damage is a central theme. In contrast with traditional structural engineering, which focuses on forces and displacements, performance-based engineering entails the consideration of seismic consequences in terms of direct and indirect cost of damage to structures. To account for unavoidable uncertainties in such predictions, a probabilistic approach is adopted in this thesis. Specifically, a methodology is proposed that is based on reliability analysis in conjunction with probabilistic models. The phrase "unified reliability analysis" is employed to describe the approach. Although the framework of models generally includes hazard, structure, and consequence models, it is the damage models that are of particular concern in this thesis. In a novel approach, the visual damage at the structural component level is predicted. Importantly, such models predict "physical quantities" of damage. This is done because it is recognized that repair action selection is the central link between the predicted damage and its associated direct and indirect costs. Hence, in order to predict the repair cost and time associated with seismic events, this study puts forward damage models that are directly utilized to predict the repair action. In turn, this leads to probabilistic estimates of seismic loss by summing contributions from the components in the structure.

The probabilistic model development follows a Bayesian framework. This approach builds on linear regression theory and explicitly accounts for uncertainties. Specifically, the coefficients in the linear regression models are random variables. The probabilistic models developed in this thesis facilitate the unified reliability analysis that ultimately determines final loss probabilities. This thesis describes the overall methodology, which is generic and applicable to a wide range of

structural components, and applies it to reinforced concrete components. This specific application includes the development of a probabilistic model of crack length in reinforced concrete shear walls.

Table of Contents

List of Tables

List of Figures

Acknowledgments

I would like to express my sincere gratitude to my supervisors Dr. Terje Haukaas and Dr. Kenneth Elwood for their valuable support. Their encouragement and guidance from the initial to the final stage of the research provided me deep understanding of the subject.

It is also my pleasure to thank all the members of the infrastructure risk strategic research group, Majid Baradaran Shoraka, Alejandro Bohl, Dr. Stephanie Chang, Dr. Ricardo Foschi, Edwin Guerra, Mojtaba Mahsuli, Laura Quiroz and Karthick Pathman for their insightful comments and contributions. I am also grateful to Dr. Perry Adebar, Dr. Tony Yang and Ehsan Dezhdar for their valuable input and knowledge.

I also wish to thank the Natural Sciences and Engineering Research Council of Canada for funding this project as well as the Department of Civil Engineering and the Faculty of Graduate Studies at the University of British Columbia for granting me the University of British Columbia Graduate Fellowship.

Dedications

To my mother who believes everything is possible.

1 Introduction

1.1 Objectives

In the context of performance-based earthquake engineering, this work aims at the estimation of seismic loss to reinforced concrete (RC) structures in terms of repair cost and repair time. In particular, the loss to a structure is determined based on component losses. To determine the loss in each component, it is recognized that repair action is the central link between the component damage and the associated repair cost and time. Clearly, the selection of an appropriate repair action demands the prediction of accurate quantities of damage. Hence, the objective of this work is to propose a methodology in which "visual damage" in components after occurrance of an earthquake can be predicted. For this reason, the consecutive visual damage states in each component are identified and related to structural responses determined structural analysis. As such, the proposed methodology includes a chain of analyses starting with structural responses input into "damage models" and the results of which are input into "loss models" in terms of repair cost and time. The objective of this work, nevertheless, is to perform such consecutive analysis in a rather new approach which includes the application of probabilistic models.

The probabilistic models of damage and loss proposed herein are rather new to the application of performance-based seismic engineering. Such models are based on the Bayesian approach which extends on the linear regression theory. The procedure includes iterations between the Bayesian inference and diagnostics. Undoubtedly, accurate predictions of damage and the subsequent losses involve significant and unavoidable uncertainties. For this reason, the probabilistic models herein are based on the application of Bayesian notion of probability to account for sources of uncertainties.

To facilitate the understanding of the proposed methodology, an initial objective is to review performance-based earthquake engineering in general and the various models of damage and loss existing in the literature. Subsequently, this work aims at illustrating in depth the proposed methodology and probabilistic model development procedure. Implementation of the proposed methodology on light-to-moderate damage to flexural RC shear walls further illustrates the methodology. By utilizing a database of analytical results on shear walls, this study aims at developing a probabilistic damage model of crack length.

In summary, the objectives of this work include:

- Propose a new probabilistic approach based on the Bayesian notion of probability for the development of seismic damage and loss models;
- Propose a methodology that determines "visual damage" in RC components by several "quantity-type" and "threshold-type" probabilistic models;
- Relate structural responses to estimates of loss in terms of repair cost and time;
- Develop a database of analytical records of crack length in RC ductile shear walls; and
- Develop a continuous probabilistic model of crack length for RC shear walls.

1.2 Motivation

Several factors motivate the application of probabilistic models in the prediction of seismic damage and loss to structures in thesis. First is the existence of uncertainties. Significant uncertainty including those aleatory (irreducible) in nature and epistemic (reducible) exists in all the stages of performance-based seismic analysis, from hazard analysis to the subsequent loss. Clearly, deterministic models of damage and loss do not account for the sources of uncertainties and hence are not fully representative of the actual earthquake consequences. The second motivating factor is in the characterization of uncertainties. Several methodologies are proposed in the literature to account for uncertainties through probabilistic manners. Still, such methods do not distinguish between aleatory and epistemic uncertainties. In contrast, in the probabilistic models in this thesis the aleatory uncertainties in input random variables are differentiated from the epistemic uncertainties in model parameters.

The other motivation is to put forward probabilistic models that produce a unique damage scenario, rather than a probability. This contrasts with widely used models that produce a conditional probability rather than a unique result. In this thesis, instead of performing reliability methods in each stage of the analysis, a single reliability method- such as FORM- can be used in conjunction with probabilistic models to predict damage and loss. Herein, the probabilistic models essentially simulate an outcome of reality for given values of model parameters and responses. This is highly desirable in the context of the reliability analysis approach that is adopted in this work. In this framework, many models for hazard, structure, and consequences interact. Instead of passing conditional probabilities from one model to another, this thesis adopts the viewpoint that all uncertainty is described by random variables that are input to the models.

For given values (realizations) of these random variables, the models produce a unique result. It is also noted that the type of probabilistic model that is developed in this thesis provides added insight compared with those that only provide a probability as output. Deterministic—or simulated—measures of damage and loss provide better understanding of actual performance. Physical insight gained from probabilistic model is an important motivation in this thesis.

The literature includes extensive research on the seismic behaviour of ductile RC shear walls, particularly at failure. This is important when designing walls considering survival limit states. On the other hand, less research has been conducted to predict the early levels of damage associated with small to moderate earthquakes. This is also significant because considerable damage in terms of cracking and spalling occurs in walls though the structure is still safe for use. Currently, no model is available in the literature determining early damage in shear walls. As such, the final chapters of this work are intended to develop a probabilistic model that predicts the total length of early cracks in shear walls. Indeed, this is in the context of performance-based engineering in which the focus is not solely on collapse prevention but also on the prediction of actual performance.

1.3 Scope

The proposed methodology is applicable to any RC component. This is discussed in Chapter 3, in which the statistical analysis and Bayesian inference are explained as part of the generic methodology of developing probabilistic damage and loss models. Although this allows the construction of a library of damage and loss models for various RC components, this work narrows its scope to RC shear walls.

To illustrate the implementation of the proposed methodology, a damage model for RC shear walls is developed. Due to the different structural mechanics involved in the occurrence of cracks in squat and ductile walls, this work further narrows its focus on ductile walls with ductility ratio (ratio of maximum displacement to yield displacement) greater than 3 and height-to-width ratio between 2.5 to 5. In addition, the reversed cyclic analysis used to develop the database of analytical records of crack length is a time-consuming approach. Hence, in order to reduce the number of analyses, only selected design variables are varied among walls to create the database.

Although the proposed methodology includes the development of repair cost and time models for the intended damage model, such loss models are not included in the scope of this work. The probabilistic model development procedure for both models is similar.

1.4 Organization of thesis

The remainder of this thesis is organized as follows:

Chapter 2 provides a literature review on the growth of seismic design from the current code perspectives to the next-generation performance-based engineering. This chapter also includes a review on the approaches to the prediction of seismic consequences. This serves as background to the development of a damage probabilistic model for shear walls presented in the final chapters.

In Chapter 3, a unified reliability analysis approach is first described for which the proposed probabilistic models are intended. This chapter also illustrates the development of generic probabilistic models of visual damage, repair cost and repair time. The mathematical modeling of probabilistic models and the application of the Bayesian notion of probability are demonstrated.

The following Chapters of 4 and 5 focus on the implementation of the proposed methodology and in particular the development of a visual damage model for RC ductile shear walls. Chapter 4 describes a database of analytical results of crack length in walls from analysis of various ductile shear walls designed based on the Canadian Standard Association (CSA Standard A23.3-4 2006). The analytical modeling and analysis procedure are presented in depth in this chapter. In Chapter 5, a probabilistic model of crack length is developed along with the detailed description of the Bayesian approach. The final results in terms of predictions of the total crack length in walls are shown and compared with the analytical results. Finally, Chapter 6 includes conclusions obtained from this work along with recommendations for the future work.

2 Literature Review

2.1 The growth of performance-based seismic engineering

The objective in the current seismic design approaches prescribed by codes is to preserve life safety and avoid the failure of structures. To achieve these objectives, code documents are based on conservative formulations providing minimum limitations on the strength and stiffness of structures. Such limitations are to make sure structures will have acceptable performance for the designed level of earthquakes. The well-known equation for the calculation of the base shear common in all codes is shown in Eq. (1) (Paulay and Priestley 1992):

$$V_b = C_{T,S,\mu,p} \sum_1^N W_{tr} \qquad \text{Eq. (1)}$$

in which the first term on the right side is the factor accounting for seismicity of the zone, building period, T, soil type S, assigned ductility capacity, μ and the acceptable probability of exceedance, p. W_{tr} is the total floor weight at level r and N refers to the number of stories. Although based on empirical and conservative calculations, Eq. (1) does not directly account for the "performance" of the structure. In other words, following the codes implies the belief that life safety and collapse prevention under severe earthquakes are achieved by the requirements. It also reveals that damage to the structures will be in acceptable range under smaller earthquakes following the strength and deformation limitations imposed by the codes. Nevertheless, still the compliance of the structure to the intended performance remains uncertain under a future earthquake (Bohl 2009).

It is also believed that following code requirements means accounting for the inherent uncertainties. Indeed, uncertainties involved in structural modeling and the level of applied

demand are accounted for in code provisions, both explicitly and implicitly. The safety coefficients used to reduce capacity and increase demand are explicit accounts of uncertainty. On one other side, conservative formulations used in the codes for engineering modeling and assumptions treat uncertainties implicitly (Haukaas and Bohl 2009). Although these safety factors lead to safe design of structures, still more economical design might be achievable if the actual performance of structures is predicted a priori.

The prediction of actual performance also helps the designers when designing structures based on selected performance objectives. Indeed, this is the central theme of the current performance-based engineering. At present, the performance is defined in terms of structural responses. First, for the selected performance different hazard levels are identified. These are usually defined in terms of the probability of exceedance in a certain period of time are considered. For the selected level of hazards, the structural responses are determined in terms of the most appropriate engineering demand parameter (EDP), to be defined shortly, such as drift ratio (Porter 2003). Then several limits are imposed by the guidelines on the responses to keep them below predefined thresholds in order to have a conservative design. The well-known approach in this regards is proposed by FEMA, the Federal Emergency Management Agency (FEMA 356 2000). In this approach, a target performance such as immediate occupancy, life safety or collapse prevention is preselected. The guideline includes measures of structural responses, such as drift ratio, being correlated with the discretely defined performance levels. Given the level of seismic hazard and the structural model, the structure is then designed to meet the selected level of performance (FEMA 445 2006).

Figure 2.1 Performance levels in FEMA 356

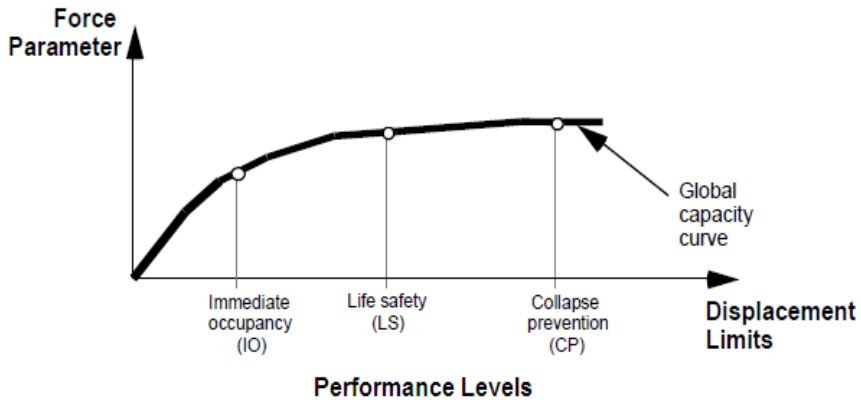

Though such determination of performance is readily implemented in engineering practice, some owners and stakeholders seek additional information regarding the performance of their structures (Haukaas 2008). In particular, decision makers are more concerned about the future loss to the structure as a result of an earthquake. Such loss varies from direct economic loss to downtime of the structure and casualties. One advantage of this is in cost-benefit analysis carried out in order to evaluate different design alternatives upon the availability of loss estimations during the design stage (Bozorgnia and Bertero 2004). The pioneering approach in this regard is the PEER integral approach, proposed by the Pacific Earthquake Engineering Research Center. Similar methods are also proposed by some other institutions such as FEMA in collaboration with ATC (FEMA 445 2006). These approaches have similar formulations, following the chain of consequences from seismic hazard to structural response, damage prediction and loss estimation (Eq. (2)). For a given level of seismic hazard and structural model, EDPs are determined from structural analysis. For the given values of EDPs, measures of damage in the structure are then determined. Finally loss values associated to the damaged structure are determined for the given measures of damage. To account for the uncertainties involved in all the

stages of the analysis, such methods predict earthquake consequences in a probabilistic manner. Clearly, prediction of seismic consequences involves significant uncertainties, both aleatory (irreducible) and epistemic (reducible). In hazard analysis, for example, there is uncertainty in the selection of the ground motions, peak ground accelerations and seismic intensity. Uncertainties also exist in structural modeling and assumptions, for instance, in selecting the damping of the structure, determination of actual stiffness, *etc*. Significant uncertainty is also involved in the prediction of damage to components given the variability in the component actual response and non-linear material behaviour. Variability in labour and material cost, labour hour rate, inflation, demand surge, *etc*. are also the sources of uncertainties in the estimation of repair cost and time. The formulations essentially include conditional probabilities in conjunction with the total probability theorem. For a given earthquake intensity measure, a resulting structural response measure, a resulting damage measure and a resulting decision variable, the theorem of total probability is applied three times. The methodology is described in a closed form equation (Cornell and Krawinkler 2000):

$$F(dv) = \iiint F(dv|dm)dF(dm|edp)dF(edp|im)f(im) \qquad \text{Eq. (2)}$$

in which *dv* is the decision variable in terms of losses, *dm* is the damage measure, *edp* is the engineering demand parameter and *im* is the intensity measure. *F(dv|dm)* is the conditional probability of exceeding a loss quantity *dv* given a damage value *dm*. *F(dm|im)* is the conditional probability of exceeding *dm* value given an intensity measure *im*. Finally, *f(im)* is the probability density function of *im*. Solution to the above equation requires the development of several fragility functions which relate *edp* to *im*, *dm* to *edp* and finally *dv* to *dm*. The final result is the

cumulative distribution function of loss defined based on the greatest interest for decision making in terms of repair cost, downtime, casualties, *etc*. (Porter 2003).

Although the above method has various advantages including accounting for uncertainties through probabilities, it has some drawbacks. Indeed, to develop the continuous probability functions required to carry out the integration, various simplifications and assumptions are required. Various researchers have worked on proposing analytical and discrete methods to implement Eq. (2) without the need to solve the triple-integration. Some of these approaches are discussed in the next section.

2.2 Prediction of seismic consequences

Analytical methods were in focus for decades when earthquake consequences in terms of damage are sought. Various structural characteristics are employed for this purpose including stiffness degrading damage models (Banon et al. 1981) and structural eigen-frequencies and mode shapes (Petryna and Krätzig 2005). To determine damage, several damage types such as cracking and buckling in a RC structure are identified to which structural responses are correlated. These approaches are, however, less applicable when more specific information on damage is needed. In other words, the drawback of such methods is in the difficulty of relating the structural responses to physical quantities of damage such as length of cracking and area of spalling in RC. Another approach is the application of damage indices. Weather deformation-based, energy-based or a combination of the two, damage indices determine damage in terms of a non-dimensional value between zero (no damage) and unity (complete failure). The best-known approach for RC components is that of Park and Ang (1985) shown in Eq. (3):

$$D = \frac{\delta_m}{\delta_u} + \beta_e \frac{\int dE}{F_y \delta_u} \qquad \text{Eq. (3)}$$

This approach is based on the combination of deformation (the first term on the right side of the equation) and energy dissipation (the second term) of the component determined by non-linear response history analysis. δ_m is the maximum response deformation and δ_u is the ultimate deformation capacity under static loading. β_e is the coefficient for cyclic loading, F_y is the calculated yield strength and dE is the incremental absorbed hysteresis energy. The result is then correlated with measures of damage defined by discrete damage states. The damage states divide the continuous development of damage in a structure to a few broad categories such as “slight

damage" or "complete damage", as shown in Table 2.1. Williams and Sexsmith (1995) provide a comprehensive review of seismic local and global damage indices developed in the literature for reinforced concrete structures. Most damage indices including Eq. (3) however have complex formulae and require cumbersome non-linear structural analysis not commonly used in practice. The non-dimensional index is not also a clear indicative of the actual performance (FEMA 445 2006).

Table 2.1 Correlation of damage indices to measures of damage (Park et al. 1985)

$D < 0.1$	No damage or localized minor damage
$0.1 \leq D < 0.25$	Minor damage- light cracking throughout
$0.25 \leq D < 0.4$	Moderate damage- severe cracking, localized spalling
$0.4 \leq D < 1.0$	Severe damage- crushing of concrete, reinforcement exposed
$D \geq 1.0$	Collapse

The application of empirical models is an alternative approach for the determination of seismic consequences. Empirical models are constructed based on observed damage and loss to buildings from past earthquakes. The well-known approach in this regard is that of ATC 13 (1985), developed by the Applied Technology Council and funded by the Federal Emergency Management Agency (FEMA). This guideline considers industrial, commercial, residential, utility and transportation facilities in California. In this approach, damage is defined by damage probability matrices, predicting the excepted percentage of damage to a given structural type for a given seismic intensity. Such matrices are developed for 78 facility classes. The approach also provides estimates of the time required to restore the damaged facilities and the information necessary to determine regional loss. The information provided in this report is collected based

on expert opinion. Hence, it is highly subjective and clearly only applicable to structures with similar characteristics (Lang 2002).

Recently the application of fragility curves has been widespread. Fragility curves are essentially based on conditional probability functions. Damage fragility curves, for instance, determine the conditional probability of being in a damage state for a given ground shaking intensity or structural response (Figure 2.2). When a structural response is used as an input, this response is usually selected as the most significant EDP, such as drift ratio for structural components. Such probability curves are developed based on experimental data and expert opinion and by assuming a distribution type (usually lognormal) to the observed data. In return, the damage state is linked with a cost estimate, either in form of loss fragility curve or lookup tables. An example of the application of fragility curves in the context of PEER approach is the methodology proposed by Yang et al. (2009). In this approach, various scaled ground motions are used to generate EDPs by a number of non-linear dynamic analyses and artificially generated random variables. Next, the various building components are organized into performance groups, each associated with a peak EDP. Each performance group is also associated with a set of fragility curves, providing the probability of exceeding a damage state in the component given the level of EDP. Lookup tables are then used to determine the cost associated with the repair of each damage state; however, in order to estimate a final loss value, a uniform random number generator is used to determine the damage state for a given level of demand. The application of fragility curves is also proposed by some other researchers. In the approach taken by Pagni and Lowes (2006), various discrete damage states for older RC beam-column joints are identified, based on which the necessary repair methods are selected. The fragility curves are obtained based on existing experimental data on older RC beam-column joints. For given values of EDPs, the fragility curves predict the

probability of requiring a certain repair method. For each repair method, the cost of repair is determined as a product of the type of damage, size of the component and the unit cost of repair including cost of labour, material, equipment, *etc*. Markups such as contractors' profit and overhead are then applied on the total repair cost of the building.

Figure 2.2 Damage state fragility curves

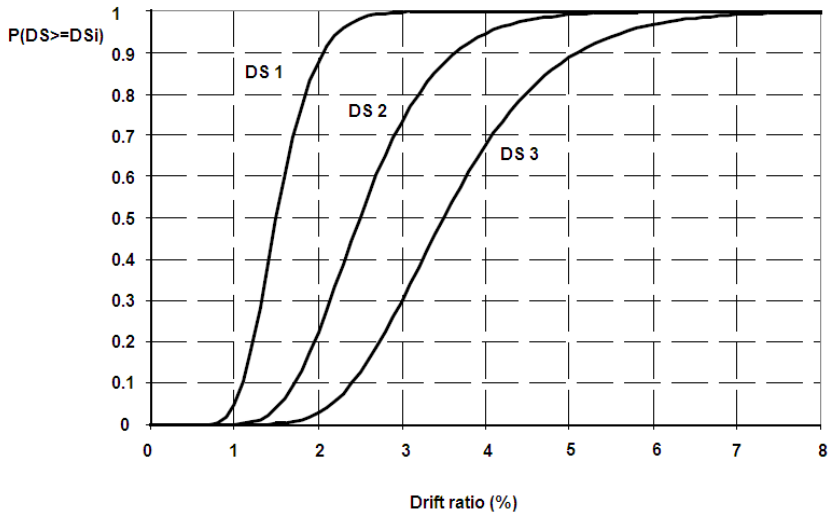

The application of the fragility curves discussed above has the advantage of providing a visual representation of the probabilities associated with various damage states and the corresponding loss estimates. Nevertheless, the application of fragilities for the prediction of seismic consequences lacks in some ways. First, damage is identified discretely for all components though it is a continuous phenomenon for many structural types such as RC. Second, fragilities provide results in form of probabilities instead of deterministic. It is recognized that this is to account for the existing uncertainties. However, alternative approaches exist which are capable of providing unique results while also accounting for the sources of uncertainties. These are the

unique features of "probabilistic models". Examples of probabilistic models developed in the literature are the models for deformation and shear capacity by Gardoni et al. (2002b) for circular RC columns subjected to reverse cyclic loading. Zhu et al. (2007) also developed probabilistic models at the onset of lateral strength degradation and axial load failure for rectangular RC columns under seismic loading tested in the past. Ramamoorthy et al. (2006) constructed probabilistic seismic demand models to predict the maximum inter-story drift in RC frame buildings.

Construction of probabilistic models to predict seismic damage and loss is the core objective of this work. Hence, the general appealing features of probabilistic models and the model development procedure are discussed in depth in the chapter Proposed Methodology.

3 Proposed Methodology

3.1 Unified reliability analysis

The unified reliability analysis (URA) (Haukaas 2008), for which the proposed damage and loss models are intended, addresses performance-based engineering. The URA is the central theme of the ongoing work by the infrastructure risk research group (www.inrisk.ubc.ca), at the University of British Columbia, Vancouver, BC. Similar to the PEER approach, the objective of the URA is two-fold. On one side, it relates seismic hazard analysis to estimates of loss, in particular, to direct and indirect cost and repair time. On the other side, the URA aims at accounting for the sources of uncertainties involved in all the stages of analysis from seismic hazard to loss estimation. Nevertheless, the URA takes a different approach. Indeed, there are two major differences between the URA and the PEER approach. First, continuous "probabilistic models" are used instead of conditional probability functions. Second, a single reliability method, instead of the triple integral, is sufficient to carry out the analysis and determine the final loss probability curve (Haukaas 2008).

To further illustrate the approach taken by the URA, the classical reliability analysis is first reviewed. Such analysis is based on the formulation of a limit state function, $g(\mathbf{x})$, in which $\mathbf{x}$ is the vector of random variables. The limit state function is formulated such that a negative value indicates the failure state. In other words:

$$\begin{cases} g \leq 0 \text{ indixcates the failure state} \\ g > 0 \text{ indicates the safe state} \end{cases} \qquad \text{Eq. (4)}$$

In the context of the URA, the desired value is in terms of loss (e.g. repair cost) and so the limit state function reads:

$$\mathrm{g}(dv, \mathbf{x}) = DV(\mathbf{x}) - dv \qquad \text{Eq. (5)}$$

in which *DV* is the perceived loss (e.g. direct repair cost) and *dv* is a selected threshold value of loss. The goal of reliability analysis is then to determine the probability that the perceived loss is less than the threshold:

$$p = \int_{-\infty}^{\infty} \dots \int_{-\infty}^{\infty} I(\mathbf{x}) f(\mathbf{x}) \mathrm{d}\mathbf{x} \qquad \text{Eq. (6)}$$

$$I(\mathbf{x}) = \begin{cases} 1, & g(\mathbf{x}) \leq 0 \\ 0, & g(\mathbf{x}) > 0 \end{cases} \qquad \text{Eq. (7)}$$

In Eq. (6), $f(\mathbf{x})$ is the joint probability distribution (PDF) of random variables. Implementing Eq. (5) in Eq. (6) results in the probability that the selected threshold value, *dv* exceeds $DV(\mathbf{x})$. The cumulative distribution function, determining the probability that the outcome is less than or equal to *dv*, is then formulated as (Haukaas et al. 2010):

$$F(dv) = p(dv) = \int_{-\infty}^{\infty} \dots \int_{-\infty}^{\infty} I(dv, \mathbf{x}) f(\mathbf{x}) \mathrm{d}\mathbf{x} \qquad \text{Eq. (8)}$$

Eq. (8) is the essence of the URA, leading to the same result of Eq. (2). To solve the above equation, a reliability analysis is carried out with a series of sequential probabilistic models, starting with hazard models to building models, visual damage models, repair selection models and finally loss models. These models, in contrary with what their name "probabilistic" connotes, do not result in a probability value but determine unique results. Essentially, probabilistic models are in terms of a set of explanatory functions of random variables. Each probabilistic model takes input variables from the preceding model in the chain and provides

output variables for the subsequent model. The URA approach is further illustrated in Figure 3.1. Starting with earthquake hazard models, location and magnitude realizations are input to determine the site intensity realizations necessary for structural analysis by the building models. The resulting realizations of structural responses- such as drift ratio- are used in the succeeding visual damage models. These models, developed based on engineering mechanics, are able to quantify the visual damage in each component of the structure. Visual damage models are essentially developed for all components in a building including structural and non-structural components. The predicted measures of damage in each component are then utilized in the repair selection models. The repair selection models, which are the central theme of this work, assign the appropriate repair action to each component. Having the repair action selected, the loss including the direct repair cost and the time associated to repair is then determined. The summation of component losses results in the total loss to the structure.

Random variables, which represent uncertainties, are input to the probabilistic models during each iteration of the analysis (Haukaas 2008). Indeed, both aleatory (irreducible) and epistemic (reducible) uncertainties are involved throughout the analysis. In hazard analysis, for example, there is uncertainty in the selection of the ground motions, peak ground accelerations and seismic intensity. Uncertainties also exist in structural modeling and assumptions, for instance, in selecting the damping of the structure, determination of actual stiffness, *etc*. Significant uncertainty is also involved in the prediction of damage to components given the variability in the component actual response and non-linear material behaviour. Variability in labour and material cost, labour hour rate, inflation, demand surge, *etc*. is also represent source of uncertainty in the estimation of repair cost and time.

Figure 3.1 Flow of information through models in a unified reliability analysis

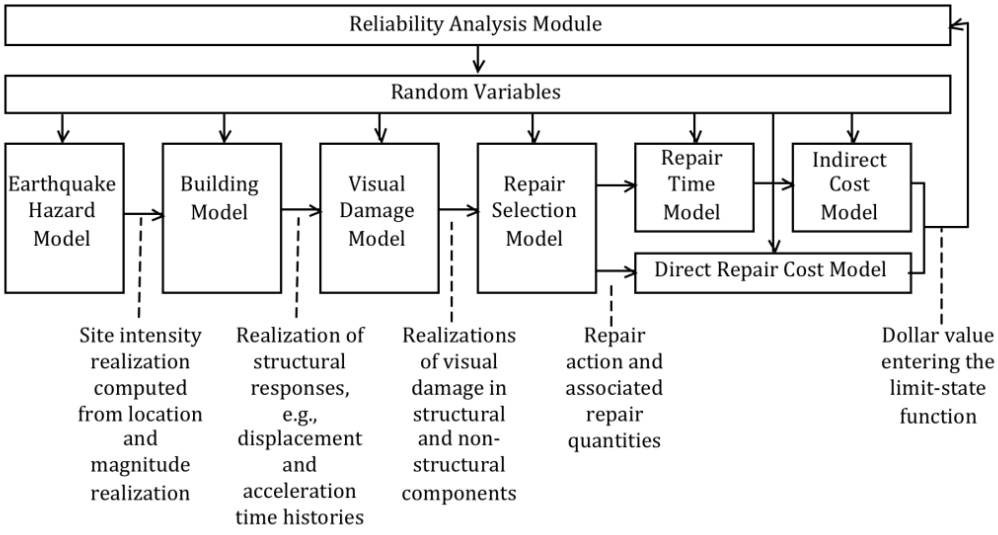

The sequential flow of information from each probabilistic model to the next and the continuous nature of the probabilistic models facilitate the reliability analysis to be carried out. For a certain loss threshold and given input random variables at each analysis stage, a single reliability analysis method such as first- and second- order reliability methods (FORM and SORM) or Monte Carlo sampling can be performed to develop the probability loss curve (Haukaas and Bohl 2009).

In the definition that is adopted in this thesis, probabilistic models are essentially input-output-type models. Each probabilistic model (e.g. a damage model) takes three categories of input parameters: a) input values from the preceding model (e.g. drift ratio of a shear wall from the building model); b) random variables that represent quantifiable physical variables (e.g. ratio of flexural reinforcement); and c) random variables that represent the model parameters. In turn, the model determines a unique output (e.g. measure of cracking). This is also illustrated in Figure 3.2.

Figure 3.2 Probabilistic analysis model

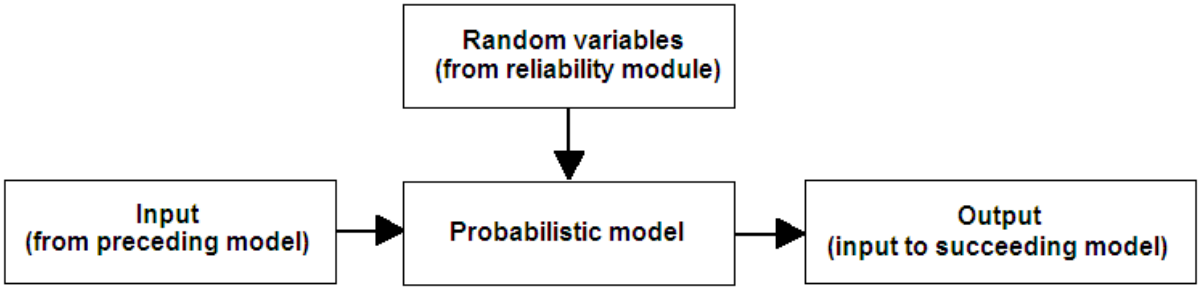

Generally, the type of probabilistic model developed depends on the characteristics of the problem in hand. For instance, models can be either discrete or continuous depending on the nature of the desired output. A continuous model is best suited to quantify the continuous increase in spalling of cover concrete in RC components subjected to seismic loads. On the other hand, discrete models are better representative of the progression of damage in steel components representing the onsets of yielding, buckling and fracture. Models are also diverse in dimensions ranging from uni-variate models, for a scalar value of regressand, to multi-variate models for a vector of regressands. The structure of the models also varies from algebraic to algorithmic expressions. In algebraic expressions, variables are explicitly included, such as the classical linear regression models. In algorithmic models, on the other hand, random variables are implicitly accounted for (e.g. from a finite analysis model). If algebraic models are sought, the models might take various forms such as linear or non-linear. The most common category, by far, is the linear form (Haukaas et al. 2010). The probabilistic models of damage and loss in this work are linear in form. Hence, only the methodology related to the development of linear models is described herein.

3.2 Linear model development procedure

3.2.1 Ordinary least squares inference

Development of a linear probabilistic model is based on the classical linear regression analysis and its basic principle of estimation through ordinary least squares method. To illustrate the methodology, first consider a classical regression analysis by which a model of visual damage is sought. In the following, the dependent variables (regressands), such as measures of damage, are denoted y and are paired with the independent variables (regressors), such as material properties and structural responses, called in the vector x. Also note that the scalar values (e.g. y) are represented in here by regular font letters whereas bold letters are used for a matrix of variables (e.g. $\mathbf{X}$). The number of paired observations on y and x is denoted n. Hence, the vector of observed responses, $\mathbf{y}$, is n-dimensional, while the observations of the independent variables are collected in the matrix $\mathbf{X}$, which has n rows. The matrix $\mathbf{X}$ has k number of columns; one for each of the k regressors. The relationship between $\mathbf{y}$, the vector of observations on damage and $\mathbf{X}$, the matrix of measurable variable, is then given by:

$$\mathbf{y} = f(\mathbf{X}) + \boldsymbol{\varepsilon} \qquad \text{Eq. (9)}$$

For a linear relationship, the above equation takes the form:

$$y = (\theta_1 x_1 + \theta_2 x_2 + \cdots + \theta_k x_k) + \varepsilon \qquad \text{Eq. (10)}$$

in which $\boldsymbol{\theta} = (\theta_1, \theta_2, ..., \theta_k)$ is the vector of unknown model parameters and ε is the model error. In classical regression analysis, a linear model is developed by determining point estimates of $\boldsymbol{\theta}$ values and fitting the right side of the Eq. (10) to the observations, $\mathbf{y}$, while lumping all the errors

in $\boldsymbol{\varepsilon}$. This is performed by minimizing the sum of the observed squares errors $\|\varepsilon\|^2 = \varepsilon_1^2 + \varepsilon_2^2 + \ldots + \varepsilon_n^2$, which is also equal to:

$$\|\varepsilon\|^2 = (\mathbf{y} - \boldsymbol{\theta}\mathbf{X})'(\mathbf{y} - \boldsymbol{\theta}\mathbf{X}) \qquad \text{Eq. (11)}$$

Notice it is assumed $\boldsymbol{\varepsilon} \sim (\mathbf{0}, \sigma^2\mathbf{I}_n)$. That is, ε values have zero mean, standard deviation σ and are uncorrelated to each other denoted by n dimensional unit matrix $\mathbf{I}_n$. A minimum of $\|\varepsilon\|^2$ will always exist due to being a real valued and differentiable function (Rao and Toutenburg 1999). Setting the first derivative of Eq. (11) to zero yields:

$$(\mathbf{X}'\mathbf{X})\widehat{\boldsymbol{\theta}} = \mathbf{X}'\mathbf{y} \qquad \text{Eq. (12)}$$

and assuming $\mathbf{X}$ is full rank k, that is the number of observations is greater than the number of regressors, $n>k$, then $\mathbf{X}'\mathbf{X}$ is non-singular and the unique solution is:

$$\widehat{\boldsymbol{\theta}} = (\mathbf{X}'\mathbf{X})^{-1}\mathbf{X}'\mathbf{y} \qquad \text{Eq. (13)}$$

The error term, ε, has the variance:

$$\widehat{\sigma}^2 = \frac{1}{\mathrm{n-k}}\left(\mathbf{y} - \mathbf{X}\widehat{\boldsymbol{\theta}}\right)'\left(\mathbf{y} - \mathbf{X}\widehat{\boldsymbol{\theta}}\right) \qquad \text{Eq. (14)}$$

To this end, a classical linear regression model is developed by determining the point estimates of $\boldsymbol{\theta}$ values and the associated variance. The Bayesian inference, which is used to develop the probabilistic models in this thesis, extends the classical linear regression by assuming a joint probability distribution for the model parameters, $\boldsymbol{\theta}$, and the model error, $\boldsymbol{\varepsilon}$ (Box and Tiao 1992). In other words, the model parameters are assumed as random variables with associated statistical parameters. This is illustrated in the following section.

3.2.2 Bayesian inference

A uni-variate probabilistic model without a deterministic model term takes the form (Gardoni et al. 2002b):

$$D(\mathbf{x}, \boldsymbol{\Theta}) = \gamma(\mathbf{x}, \boldsymbol{\theta}) + \sigma\varepsilon \qquad \text{Eq. (15)}$$

in which

$$\gamma(\mathbf{x}, \boldsymbol{\theta}) = \sum_{i=1}^{p} \theta_i h_i(\mathbf{x}) \qquad \text{Eq. (16)}$$

In the above equations, $\boldsymbol{\Theta} = (\boldsymbol{\theta}, \sigma)$, $\boldsymbol{\theta} = (\theta_1, \theta_2, ...)$ and σ is the standard deviation of the model error. The term $h_i(\mathbf{x})$, called an explanatory function, is a function based on the independent variables. The selection of explanatory functions can be based on engineering mechanics, judgement or intuition. Though the explanatory functions in θ values are linearly added, they can be of non-linear form in **x** variables (Gardoni et al. 2002b).

In contrast to the classical regression analysis in which all the model error is lumped in ε, the Bayesian inference distinguishes between aleatory and epistemic uncertainties. Aleatory uncertainties, irreducible and inherent in nature, are represented in the independent variables, **x**, and partly in ε. On the other hand, epistemic uncertainties, which are reducible and due to lack of knowledge, are represented in the unknown model parameters, $\boldsymbol{\theta}$, and partly in term ε (Gardoni et al. 2002b). The unknown model parameters are estimated by "Baye's Theorem". To illustrate this theorem, first consider the previously defined set of dependent observations, $\mathbf{y}' = (y_1, y_2, ..., y_n)$ and the set of unknown model parameters, $\boldsymbol{\theta} = (\theta_1, \theta_2, ...)$. According to the Baye's theorem, the conditional probability of $\boldsymbol{\theta}$ for given observations of **y** is determined by:

$$p(\boldsymbol{\theta}|\mathbf{y}) = \frac{p(\mathbf{y}|\boldsymbol{\theta})p(\boldsymbol{\theta})}{p(\mathbf{y})} \quad \text{with} \quad p(\mathbf{y}) \neq 0 \qquad \text{Eq. (17)}$$

For continuous $\boldsymbol{\theta}$, $p(\mathbf{y})$ can be defined in terms of Eq. (18) in which $E_{\boldsymbol{\theta}}[p(\boldsymbol{\theta})]$ is the mathematical expectation of $p(\boldsymbol{\theta})$ (Gardoni 2002a):

$$p(\mathbf{y}) = E_{\boldsymbol{\theta}}[p(\mathbf{y}|\boldsymbol{\theta})] = \kappa(\mathbf{y})^{-1} = \int p(\mathbf{y}|\boldsymbol{\theta})p(\boldsymbol{\theta})d\boldsymbol{\theta} \qquad \text{Eq. (18)}$$

Using Eq. (18), Eq. (17) can be rewritten as:

$$p(\boldsymbol{\theta}|\mathbf{y}) = \kappa p(\mathbf{y}|\boldsymbol{\theta})p(\boldsymbol{\theta}) \qquad \text{Eq. (19)}$$

in which $p(\boldsymbol{\theta})$ is the prior distribution of $\boldsymbol{\theta}$, $p(\boldsymbol{\theta}|\mathbf{y})$ is the posterior distribution of $\boldsymbol{\theta}$, $p(\mathbf{y}|\boldsymbol{\theta})$ is the conditional probability of the observations given the values of model parameters, also called the likelihood function, and κ is a normalizing constant insuring the result of integration in Eq. (19) leads to unity. The prior distribution represents the current state of knowledge on $\boldsymbol{\theta}$ and posterior distribution determines the updated state of knowledge on $\boldsymbol{\theta}$. In essence, knowledge on $\boldsymbol{\theta}$ can be updated every time new information on $\mathbf{y}$ is available. In other words, if the current knowledge is represented by:

$$p(\boldsymbol{\theta}|\mathbf{y}_1) \propto p(\mathbf{y}_1|\boldsymbol{\theta})p(\boldsymbol{\theta}) \qquad \text{Eq. (20)}$$

and a new set of information, $\mathbf{y}_2$, becomes available, the posterior distribution of $\boldsymbol{\theta}$ can be updated by:

$$p(\boldsymbol{\theta}|\mathbf{y}_1, \mathbf{y}_2) \propto p(\mathbf{y}_1|\boldsymbol{\theta})p(\mathbf{y}_2|\boldsymbol{\theta})p(\boldsymbol{\theta}) \propto p(\boldsymbol{\theta}|\mathbf{y}_1)p(\mathbf{y}_2|\boldsymbol{\theta}) \qquad \text{Eq. (21)}$$

Indeed, this is an appealing feature of Bayesian approach. Updating of $\boldsymbol{\theta}$ values allows the probabilistic model to be updated each time a new series of data is available. Once the posterior

distribution is established, the mean vector and variance matrix of $\boldsymbol{\Theta}$ can be determined. Since the computation of these values is not simple and requires multiple integrations over Eq. (18), the algorithm proposed by Gardoni (2002a) is followed herein.

For moderate to large sample size of observations, the posterior distribution is mainly affected by the likelihood function than the selected prior distribution of $\boldsymbol{\theta}$. There are several methods to select a prior distribution, some of which are discussed in the work by Gardoni (2002a). In cases where no information on $\boldsymbol{\theta}$ is available a priori, Gardoni suggests using a distribution which has the minimum effect on the posterior distribution. In the methodology illustrated herein, it is assumed that no prior knowledge on $\boldsymbol{\theta}$ is available. Hence, to define a prior distribution, the approach proposed by Gardoni is followed. First consider the previously sought uni-variate model with the vector of dependent observations, $\mathbf{y}$, having normal distribution:

$$\mathbf{y}|\boldsymbol{\mu}(\boldsymbol{\theta}), \sigma \sim \mathrm{N}[\boldsymbol{\mu}(\boldsymbol{\theta}), \sigma] \qquad \text{Eq. (22)}$$

in which $\boldsymbol{\mu}(\boldsymbol{\theta}) = [\mu_1(\theta_1), \mu_2(\theta_2),...]$ is the vector of the mean values of the unknown model parameters $\boldsymbol{\theta}$. To define a prior distribution, it is assumed that $\boldsymbol{\theta}$ and σ are approximately independent so that:

$$p(\boldsymbol{\Theta}) \approx p(\boldsymbol{\theta})p(\sigma) \qquad \text{Eq. (23)}$$

Assuming it is appropriate to take $\boldsymbol{\theta}$ as locally uniform, $p(\boldsymbol{\theta})$ will be equal to a constant (Gardoni 2002a). Using Jeffrey's rule (Jeffreys 1961), Box and Tiao (1992) show that the non-informative prior for the parameters $\boldsymbol{\theta}$ is locally uniform such that:

$$p(\boldsymbol{\Theta}) \approx p(\sigma) \qquad \text{Eq. (24)}$$

$$p(\sigma) \propto \frac{1}{\sigma} \qquad \text{Eq. (25)}$$

Solving Eq. (19) also requires the likelihood function, which is proportional to the conditional probability of the dependent observations given the model parameters. Remembering that for the y observations, the linear model is defined with normality assumption:

$$y = \boldsymbol{\theta}\mathbf{X} + \varepsilon \sim N(\boldsymbol{\theta}\mathbf{X}, \sigma^2\mathbf{I}) \qquad \text{Eq. (26)}$$

the likelihood function reads (Rao and Toutenburg 1999):

$$L(\boldsymbol{\theta}, \sigma^2|\mathbf{y}) = (2\pi\sigma^2)^{-n/2}\exp\left[-\frac{1}{2\sigma^2}(\mathbf{y} - \boldsymbol{\theta}\mathbf{X})'(\mathbf{y} - \boldsymbol{\theta}\mathbf{X})\right] \qquad \text{Eq. (27)}$$

To determine the posterior distribution of $\boldsymbol{\theta}$ in terms of $p(\boldsymbol{\theta}|\mathbf{y})$, it is required to combine Eq. (27) with Eq. (25). Defining s^2 in terms of:

$$s^2 = \frac{1}{\eta}\left(\mathbf{y} - \mathbf{X}\widehat{\boldsymbol{\theta}}\right)'\left(\mathbf{y} - \mathbf{X}\widehat{\boldsymbol{\theta}}\right), \quad \eta = n\text{-}k \qquad \text{Eq. (28)}$$

Box and Tiao (1992) show that for a non-informative prior with $\boldsymbol{\theta}$ and ln(σ) approximately independent and locally uniform, the joint posterior distribution of $\boldsymbol{\theta}$ and σ can be written as:

$$p(\boldsymbol{\theta}, \sigma^2|\mathbf{y}) \propto p(\sigma^2|s^2)p(\boldsymbol{\theta}|\widehat{\boldsymbol{\theta}}, \sigma^2) \qquad \text{Eq. (29)}$$

and the posterior distribution of $\boldsymbol{\theta}$ is:

$$p(\boldsymbol{\theta}|\mathbf{y}) = \frac{\left[\Gamma\frac{(\eta+k)}{2}|\boldsymbol{X}'\boldsymbol{X}|^{\frac{1}{2}}s^{-k}\right]}{\left[\left(\Gamma\left(\frac{1}{2}\right)\right)^{k}\Gamma\left(\frac{\eta}{2}\right)(\sqrt{\eta})^{k}\right]}\left[1 + \frac{(\boldsymbol{\theta}-\widehat{\boldsymbol{\theta}})'\mathbf{X}'\mathbf{X}(\boldsymbol{\theta}-\widehat{\boldsymbol{\theta}})}{\eta s^2}\right]^{-(\eta+k)/2} \qquad \text{Eq. (30)}$$

It should be noted that the covariance matrix of θ is $\eta s^2(\mathbf{X'X})^{-1}/(\eta-2)$ and the mean and standard deviation of σ are respectively $\sqrt{(\eta s^2/(\eta-2))}$ and $\sqrt{(\eta s^2/[(\eta-2)(\eta-4)])}$ (Gardoni 2002a).

As understood earlier, the aim of this work is to propose a new methodology for loss estimations in the context of performance-based earthquake engineering. Such loss values are useful in several ways. They provide additional information for cost-benefit analysis during the design stage of new structures as well as for rehabilitation and retrofit of existing structures. For these objectives, the most practical loss models are those incorporating all available information as well as accounting for sources of uncertainties. The Bayesian approach discussed above provides the methodology required to construct such models.

Step-wise elimination process

Clearly, several explanatory functions can be included while developing a probabilistic model. Though considering all the sources of information available seems to provide a comprehensive and less biased model, care should be taken in the inclusion of the inclusion of explanatory functions. First, addition of non-informative terms affects the accuracy of a probabilistic model. In other words, a non-informative explanatory function is usually associated with a high coefficient of variation (COV). Large values of COV reduce the accuracy of the model by increasing the model error. Second, addition of several explanatory functions might create a complex algebraic model. Hence, to achieve a compromisation between model accuracy and model simplicity, Gardoni et al. (2002b) propose a step-wise elimination process. In this process, the insignificant explanatory functions in model development are removed while monitoring the variations in the mean of the model error. This is performed by removing the explanatory

functions whose θ coefficients have high coefficient of variations. This elimination process is described below and it is carried out until an optimum value of the model error is obtained.

1. Identify the least significant explanatory functions in model development. This is performed by identifying the explanatory functions whose θ coefficient have the largest posterior coefficient of variation.
2. Ideally, the correlation coefficient among the coefficients of the remaining explanatory functions, $|\rho_{\theta_i\theta_j}|$, should be below 0.7. A higher value is representative of close correlation between $h_i(\mathbf{x})$ and $h_j(\mathbf{x})$. These explanatory functions can be combined by Eq. (31) to reduce one parameter in the model.

$$\widehat{\boldsymbol{\theta}}_i = \mu_{\theta_i} + \rho_{\theta_i\theta_j}\frac{\sigma_{\theta_i}}{\sigma_{\theta_j}}(\theta_j - \mu_{\theta_j}) \qquad \text{Eq. (31)}$$

3. If the posterior mean of σ after the assessing the above steps is not increased by an unacceptable amount, the model can be further reduced by returning to steps 1 and 2. Otherwise, no further reduction is possible and the obtained model is as simple as possible.

Diagnostics

In the process of developing a probabilistic model, diagnostic issues should be checked for. This is because the probability distributions of the model parameters are determined based on least square estimates. As such, the same diagnostics in classical regression analysis remain significant in the Bayesian approach. Such diagnostics are several including collinearity representing strong linear dependence between regressors; error correlation representing missing explanatory information among the data which has not been exploited in the model; non-normality of the errors representing the model errors not distributed according to normal distribution; outliers representing the observations distant from the rest of data; and heteroskedasticity representing the dependence of the model error on the values of independent variables. The last three issues are interrelated. In essence, the model errors non-normally distributed might be an indication of outliers among the data. The existence of outliers might lead to variations of model error with those of regressors which are representations of heteroskedasticity.

Several remedies exist when detecting outliers. Some researchers propose methods for removing the outliers form a database (John 1995). On the other hand, model transformations are sometimes used to stabilize the model error. The decision depends on the type of data in hand, the necessity of removing the outliers and if the outliers are the sources of non-normality and heteroskedasticity. Various forms of functions for variables y are available if model transformations are preferred. For Example, the work by Chatterjee and Hadi (2006) provides a list of transformation functions depending on the distribution type of y dependent variables.

As the importance of checking for diagnostics is understood, an iterative procedure between Bayesian inference and diagnostics should be carried out while developing a probabilistic model. Some of the diagnostics listed above are discussed in Chapter 5 when illustrating an example of probabilistic model development procedure.

3.3 Probabilistic damage and loss models

As stated earlier, two sets of probabilistic models are proposed herein. The first sets of models are the visual damage models determining the required repair actions. The second sets are the loss models for the associated cost and time of repairs. The selection of repair action depends on the extent and quantity of observed damage. As demand increases in RC components, damage grows from concrete cracking to spalling to reinforcement buckling and fracture. Accordingly, appropriate models might be threshold or quantity models. A quantity model accounts for the continuity in damage progression. An example of quantity model is shown below predicting area of spalling in RC concrete:

$$A_{spalling} = \theta_1 h_1(\mathbf{x}) + \theta_2 h_2(\mathbf{x}) + \cdots + \sigma\varepsilon \qquad \text{Eq. (32)}$$

In some cases, a deterministic model might be available for the intended measure of damage. For example, Igarashi et al. (2009) developed deterministic models predicting shear and flexural crack lengths in RC columns as a result of seismic loading. To develop such models, only the effect of horizontal reinforcement ratio is taken into account. Hence, a probabilistic model based on the available deterministic model can be constructed taking into account the effect of other engineering parameters not included in the deterministic model. Following Eq. (16), the missing variables are added to the deterministic model. Then the Bayesian approach discussed in the previous section is implemented to develop a probabilistic model. The probabilistic model base on the deterministic model of flexural crack length proposed by Igarashi et al. (2009) will then read:

$$L_f = 2N_f(B + 2\beta D) + \theta_1 h_1(\mathbf{x}) + \theta_2 h_2(\mathbf{x}) + \cdots + \sigma\varepsilon \qquad \text{Eq. (33)}$$

in which L_f is the length of flexural cracks, N_f is the number of flexural cracks in the plastic hinge zone, β is a constant and D is the depth of the column parallel to the loading direction. The explanatory functions in Eq. (33) are selected based on engineering design variables and rules of mechanics. Examples of x variables include ratio of flexural reinforcement and concrete compressive strength, *etc*.

A threshold model similar to Eq. (34), on the other hand, is used when the onset of a damage state is sought. For example, a threshold model might be chosen to predict the onset of flexural reinforcement buckling in RC vertical components:

$$\delta_{buckling} = \theta_3 h_3(\mathbf{x}) + \theta_4 h_4(\mathbf{x}) + \cdots + \sigma\varepsilon \qquad \text{Eq. (34)}$$

where δ_{buckling} is the drift ratio at the onset of bar buckling. Similar to quantity models, an available deterministic model can be used in the development of a threshold model. For the example of flexural reinforcement buckling, several deterministic models are proposed in the literature such as the model by Berry and Eberhard (2005).

To select the appropriate repair action based on the observed damage, several guidelines and manuals are available. Such guidelines provide descriptions of the repair actions along with materials and equipments necessary for repair, the method of execution as well as any limitation, if applicable. FEMA 308 (1998) provides guidelines for repair of seismic damaged concrete and masonry wall buildings. Upon the selection of a repair action, the associated direct cost of repair can be modeled as:

$$C_{repair} = \theta_5 h_5(\mathbf{x}) + \theta_6 h_6(\mathbf{x}) + \cdots + \sigma\varepsilon \qquad \text{Eq. (35)}$$

Examples of explanatory functions in a cost model include cost of material and equipment, labour cost and factors such as economy of scale, demand surge, inflation, *etc*. Similarly, the time of repair which depends on variables such as labour hours, mobilization time, *etc*. can be modeled as:

$$T_{repair} = \theta_7 h_7(\mathbf{x}) + \theta_8 h_8(\mathbf{x}) + \cdots + \sigma\varepsilon \qquad \text{Eq. (36)}$$

Clearly, development of the above models is mainly based on availability of observations and information on the contributing variables. Data for damage models can be collected from laboratory tests, previous earthquake damage records or analytical modeling and analysis. Data on associated factors to repair cost and time can be gathered from market observations and records as well as interviews with experts. A sample questionnaire is shown in Appendix A. This questionnaire is prepared for the collection of information on the factors involved in estimation of repair cost and time associated to damage in RC shear walls.

4 Methodology Implementation: RC Shear Walls

4.1 Introduction

In Chapter 3 the statistical analysis and procedure to develop probabilistic models were presented. This chapter focuses on the methodology used to collect the necessary data based on which a probabilistic damage model is developed. As mentioned earlier, the perceived damage model presents the early levels of damage including the length of cracks in RC shear walls as a result of seismic loading. The reason behind the selection of this damage state is due to the gap of research observed in the literature on the early damage behaviour of RC shear walls. For decades, the majority of research conducted on the seismic behaviour of RC walls focuses on the load-deformation response of walls and the ultimate behaviour in terms of failure modes. Examples of such studies include the research conducted by Oesterle et al. (1984), Thomson and Wallace (2004), Lefas et al. (1990), Zhang and Wang (2000) and Paulay and Priestley (1992). Nevertheless, studies are also required to predict the performance of walls in terms of early damage. Indeed, this is in the context of performance-based design to provide the decision-makers with the required knowledge on the associated losses in walls in terms of direct and indirect costs as a result of small to moderate earthquakes.

Although various tests are conducted on shear walls as part of the aforementioned research, few researchers have recorded the length and width of cracks as a function of applied load. Since the accuracy of a probabilistic model highly depends on the availability of large number of data, a database including the expected level of cracking in walls is created for this study. This database in based on wall damage data predicted by nonlinear analysis for a range of wall parameters used in practice. The development of this database is the central theme of this chapter.

In the following sections, first the various damage states corresponding to various stages of the load-deformation response of shear walls is reviewed in order to understand how damage progresses in walls. Next, the methodology to develop the database of data on cracking in walls is discussed. In particular the application of the non-linear program VecTor2 (Wong and Vecchio 2002), capable of determining cracking information in walls subjected to seismic loading, is demonstrated in detail. The results of analyses in terms of crack length as a function of applied loading history are next presented followed by investigating the accuracy of such data with observations from few experiments available in the literature.

The implementation of the presented data to develop the probabilistic model of crack length is discussed in Chapter 5. It should be noted that regardless of the approach used to collect data, from analytical methods to laboratory tests and direct recordings from previous earthquakes, the model development procedure is essentially the same.

4.2 Damage to RC shear walls

Damage mechanism is significantly affected by the behaviour mode and ductility of walls (FEMA 306 1998). Squat walls, usually with height-to-width ratio (defined herein as slenderness ratio) less than 2, exhibit a different damage response to seismic loading than those walls with greater slenderness ratio. Due to their relative cross sectional dimensions, boundary conditions and the method of shear transfer, the behaviour of squat walls is usually controlled by shear. In particular, these walls are prone to diagonal tension and compression failure and sliding shear (Paulay and Priestley 1992). On the other hand, the behaviour of slender walls is mainly controlled by flexure and the non-linear mechanism at the end portion of the wall in the plastic hinge zone. Hence, this study narrows it focus to slender walls having height-to-length ratio equal to or greater than 2.5. Ductility of walls also affects the severity of damage. Ductile walls exhibit large deformations before peak-strength and prior failure whereas brittle walls have limited deformation capacity. Ductility of walls is a function of several variables in walls including slenderness ratio, axial load ratio, flexural reinforcement ratio, *etc*. As a result, minimum displacement ductility- the ratio of maximum displacement to yield displacement- of 3 is set as a requirement for all walls considered in the database to guarantee a ductile behaviour.

ATC 58 (2009) provides general information on several damage states in ductile flexural walls based on the tests conducted in the literature. These damage states are shown in Figure 4.1 in which the images are taken from the experiments by Corley et al. (1981). The description of each damage state is also listed in Table 4.1. It should be noted that the values presented in this table refer to the maximum crack width when the wall is displaced up to the indicated end rotation. The indicated values are approximate and may not necessarily be the same for all ductile walls.

Figure 4.1 Damage states in ductile flexural walls

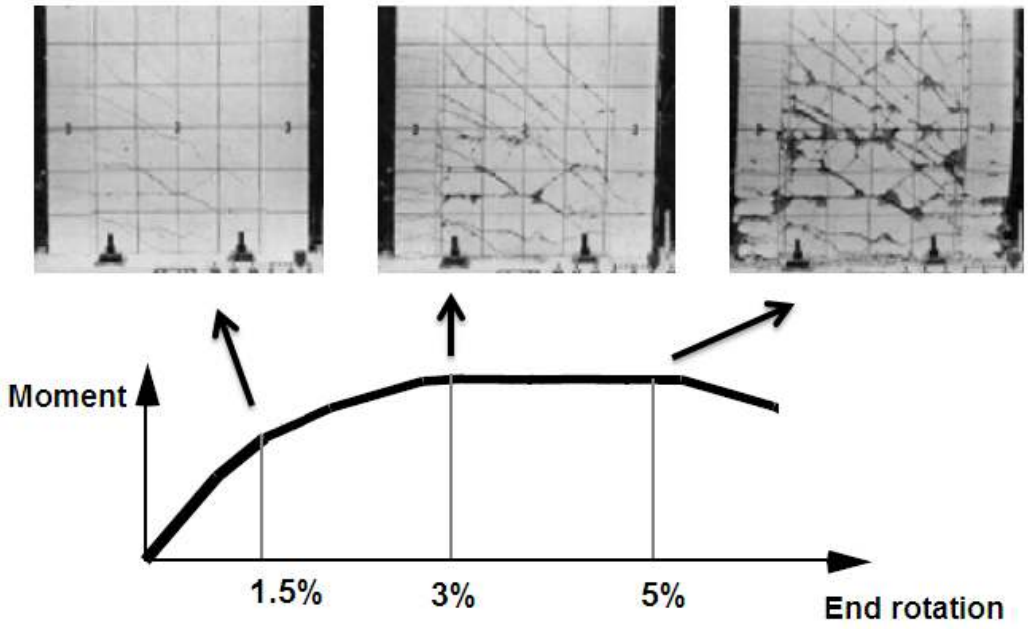

Table 4.1 Description of damage states in ductile flexural walls (ATC 58 2009)

End rotation	Damage Description
1.5%	Flexural cracks < 4.5mm Shear (diagonal) cracks < 1.5mm No significant spalling No fracture or buckling of reinforcement Not structurally significant
3%	Flexural cracks > 6mm Shear (diagonal) cracks > 3mm Moderate spalling/ loose cover No fracture or buckling of reinforcement Insignificant residual drift/shortening
5%	Maximum crack widths > 9.5mm Significant spalling/ loose cover Fracture or buckling some reinforcement Significant residual drift/shortening

As indicated in Figure 4.1, damage initiates with cover concrete cracking. The fine cracks associated with rotational demand less than 1.5% as a result of small earthquakes do not usually affect the performance of the wall. As demand increases, the cracks extend in width and length and propagate towards the core concrete. Further displacement of the wall causes the cover

concrete to loosen and spall off though significant spalling does not usually occur before reaching the post-peak response. Degradation of the response occurs after maximum strength of the wall. This is associated with core concrete crushing followed by the buckling of the flexural reinforcement and yielding and fracture of the horizontal reinforcement. At this stage of response, cracks can be as large as 9.5mm in width.

This study focuses on predicting the length of cracks during the initial range of load-deformation response up to peak strength. The maximum crack widths which occur in walls displaced to maximum displacement position are not necessarily equal to the widths of cracks after occurrance of an earthquake. This is because crack closure occurs as a result of stress redistribution when portion of the wall displacement is recovered after seismic loading reduces to zero. The cracks observed after an earthquake are referred to as residual cracks. The length of such residual cracks are the intended data for this study, considering the ultimate purpose of the proposed methodology is to determine the repair cost and time associated to damage after an earthquake occurs (Chapter 3).

The width and total length of residual cracks are the primary factors in determining the cost and time of repair of cracks. In essence, for given ranges of crack width, the total length of cracks is measured and the type of epoxy injection required for repair is selected. This method is used in the example provided in FEMA 307 (1998) for the repair of the shear walls in a two-story concrete building damaged after Northridge earthquake in 1994. FEMA 308 (1998) provides suggestions for the types of epoxy to be used for various widths of cracks observed in the various stages of response. In this study, however, the same material type is assumed considering the limited range of residual crack widths which occurs prior post-peak response. Based on the

analytical studies conducted herein, the width of such cracks ranges from 0.5 to 3mm. This is explained in detail in the following sections.

4.3 Database of analytical walls

This study focuses on the behaviour of shear walls designed in practice based on Canadian Standard Association (CSA) code requirements (CSA Standard A23.3-4 2006). As mentioned earlier, the focus is narrowed to slender walls having height-to-width ratios of 2.5 to 5 with minimum displacement ductility of 3 to assure ductile behaviour. All walls are rectangular and the method of design follows the requirements for flexural and axial loads as well as shear and torsion in Clauses 10 and 11 in CSA, respectively. Special attention is also given to the critical region at the base of the walls due to concentration of inelastic response. The requirements for seismic design are provided in Clause 21 of CSA. The design variables including concrete compressive strength, axial load ratio, flexural and horizontal reinforcement ratio, yield strength of flexural reinforcement, aspect ratio and height-to-width ratio are varied considering the permissible design ranges provided in CSA. These variables are discussed below and shown in Table 4.2. Wall NO.1 is designed as the base case compared to which the design variables are varied. In other words, this wall appears in the comparison of results in each series of wall. The properties of this wall are selected as a typical wall design in practice. All walls have length-to-width ratio of 9.8.

Concrete compressive and tensile strength

Concrete is known to crack when tensile stresses exceed the tensile strength of concrete. Although the tensile strength of concrete reduces to zero at the location of cracks, concrete continues carrying tensile stresses in between the cracks. In practical applications, concrete tensile strength is not precisely known in priori. It is usually estimated with a non-linear relation to the concrete compressive strength. This non-linearity is typically represented with various

power values. Oluokun (1991) reviews the various models developed for the relation between concrete compressive and tensile strengths in literature. Herein the effect of tensile strength is taken as proportional to the square root of concrete compressive strength. This is consistent with the conventional modulus of rupture in the CSA Standard A23.3-4 2006 standard:

$$f_r = 0.6\lambda\sqrt{f_c'} \qquad \text{Eq. (37)}$$

in which λ is equal to 1 for normal density concrete. Simultaneously, concrete compressive strength is also varied between 25-45MPa to consider the effect of concrete compressive strength. This is important considering the significant contribution of concrete compressive strength on cracks in RC.

Axial load ratio

It is widely known that axial load ratio significantly affects the response of shear walls and controls the level of damage during seismic loads. Indeed, the formation of cracks in highly dependent on the level of applied axial load. As axial compressive stress rises on the cross section of the wall, the tensile stresses causing concrete to crack reduce. Zhang and Wang (2000) conducted several tests on the effect of axial load on shear walls with various height-to-width ratios. They conclude that the occurrance of first cracks in walls is postponed proportionally with the level of axial load. In practice, shear walls are designed carrying various levels of axial load ratios. In this work, to satisfy minimum displacement ductility ratio (ratio of maximum displacement to yield displacement) of 3, axial load ratio is varied between 0-8%.

Flexural reinforcement

Tests conducted on flexural RC components reveal that as the ratio of flexural reinforcement increases, fewer cracks are observed on the surface of concrete (Adebar and Van Leeuwen 1999). This is due to increase in strength and stiffness. Nevertheless, the formation of cracks is required in RC considering their contribution in energy dissipation of the component. Still, it should be noted that significant reduction of flexural reinforcement is also not desirable. This is because it would lead to large cracks as enough reinforcement is not available to carry the tensile stresses caused during an earthquake (Paulay and Priestley 1992). Hence, limits on both maximum and minimum ratios of flexural reinforcement are provided in most design codes.

In this study, the effects of flexural reinforcement ratios in the two regions of boundary and web of the walls are taken into account separately. In practice, more flexural reinforcement is provided in the boundary region of walls relative to the web region to increase the stiffness of the walls. This might lead to unequal distribution of cracks in the two regions. In CSA, minimum ratios of reinforcement are specified for both the web and boundary regions of walls as 0.25%. For boundary regions, there is an additional requirement that the area of concentrated reinforcement is at least $0.0015 b_w l_w$, in which b_w and l_w are the width and length of the wall, respectively. A maximum of 0.06 is also provided for the ratio of reinforcement provided to the cross sectional area of walls. The yield strength of flexural reinforcement is also considered as a design variable. Since the crack width is directly related to the tensile strains in reinforcement, increase in yield strength of rebars decreases the associated tension stress, consequently decreasing the width of cracks. In practice, the range of permissible yield strength of rebars is 400-625MPa depending on the grade of steel used(CSA Standard A23.1 2009). In this study, only the most common steel grade 400W is assumed.

Horizontal reinforcement

Horizontal reinforcement provides redistribution of cracks and enhances ductility in walls (Hidalgo et al. 2002). Such effects are more significant towards the end of response where horizontal reinforcement controls flexural reinforcement buckling and fracture. Hence, the amount of horizontal reinforcement provided in walls is less significant in the initial range of response where the behaviour is more controlled by strength of walls. Nevertheless, the ratio of horizontal reinforcement is considered as a design variable in this study to evaluate its effect on controlling the width of shear cracks. The same ratio of horizontal reinforcement is assumed for both the boundary and web sections of all walls. Based on CSA code requirement, a minimum ratio of 0.25% of horizontal reinforcement should be provided in walls.

Slenderness ratio

The effect of slenderness ratio of walls on cracking is also considered in this study. Plastic hinge length in walls is not significantly affected with variations in slenderness ratio of walls. Hence, crack length remains almost constant for walls with various slenderness ratios and displaced once to the same level of displacement. Nevertheless, the non-linear cyclic analysis on the walls in this study is based increments of yield displacement. Hence, the effect of slenderness ratio is also considered due to the variations in the yield displacement of walls with various height-to-width ratios. The slenderness ratio is varied from 2.5 to 5.

Table 4.2 Design details of walls

Wall NO	f'_c (MPa)	$\sqrt{f'_c}$	γ	ρ_{lw}	ρ_{lb}	ρ_h	f_y (MPa)	h_w/l_w
1	35	5.92	5%	0.78%	1.20%	1.00%	455	3.02
2	25	5.00	5%	0.78%	1.20%	1.00%	455	3.02
3	30	5.48	5%	0.78%	1.20%	1.00%	455	3.02
4	40	6.32	5%	0.78%	1.20%	1.00%	455	3.02
5	45	6.71	5%	0.78%	1.20%	1.00%	455	3.02
6	35	5.92	0%	0.78%	1.20%	1.00%	455	3.02
7	35	5.92	2%	0.78%	1.20%	1.00%	455	3.02
8	35	5.92	7%	0.78%	1.20%	1.00%	455	3.02
9	35	5.92	8%	0.78%	1.20%	1.00%	455	3.02
10	35	5.92	5%	0.54%	1.20%	1.00%	455	3.02
11	35	5.92	5%	1.26%	1.20%	1.00%	455	3.02
12	35	5.92	5%	2.00%	1.20%	1.00%	455	3.02
13	35	5.92	5%	2.80%	1.20%	1.00%	455	3.02
14	35	5.92	5%	0.78%	1.50%	1.00%	455	3.02
15	35	5.92	5%	0.78%	2.00%	1.00%	455	3.02
16	35	5.92	5%	0.78%	2.50%	1.00%	455	3.02
17	35	5.92	5%	0.78%	3.50%	1.00%	455	3.02
18	35	5.92	5%	0.78%	1.20%	0.34%	455	3.02
19	35	5.92	5%	0.78%	1.20%	0.57%	455	3.02
20	35	5.92	5%	0.78%	1.20%	1.60%	455	3.02
21	35	5.92	5%	0.78%	1.20%	2.00%	455	3.02
22	35	5.92	5%	0.78%	1.20%	1.00%	400	3.02
23	35	5.92	5%	0.78%	1.20%	1.00%	500	3.02
24	35	5.92	5%	0.78%	1.20%	1.00%	525	3.02
25	35	5.92	5%	0.78%	1.20%	1.00%	455	2.5
26	35	5.92	5%	0.78%	1.20%	1.00%	455	3.5
27	35	5.92	5%	0.78%	1.20%	1.00%	455	4
28	35	5.92	5%	0.78%	1.20%	1.00%	455	5
29	35	5.92	5%	0.78%	1.10%	1.00%	455	3.02
30	35	5.92	5%	0.81%	1.30%	1.00%	455	3.02
31	35	5.92	5%	0.79%	1.40%	1.00%	455	3.02
32	35	5.92	5%	0.81%	1.30%	1.00%	455	3.02

f'_c = concrete compressive strength, γ = axial load ratio, ρ_{lw} = flexural reinforcement ratio in web zone, ρ_{lb} = flexural reinforcement ratio in boundary zone, ρ_h = transverse reinforcement ratio in both web and boundary zones, f_y = yield strength of flexural reinforcement in both web and boundary zones, h_w = wall height, l_w= wall length

4.4 Application of VecTor2 finite element program

In this study, VecTor2 FE program (Wong and Vecchio 2002) is used. VecTor2 is a two-dimensional non-linear program for analysis of RC membrane elements. This program is selected herein for several reasons. VecTor2 program allows the selection of various reinforcement and concrete constitutive models, which play an important role in the accuracy of the predicted response. Given the level of stresses and strains in membrane elements, VecTor2 program is also capable of determining the characteristics of the associated cracks at each stage of the analysis. Considering also the large number of walls in the database, the relatively efficient cyclic analysis of walls with respect to other FE programs is an advantage. VecTor2 analysis is based on smeared crack approach and the application of Disturbed Stress Field Model (DSFM) (Vecchio 2000). A brief review on smeared crack approach is given next before describing the analytical modeling of walls.

4.4.1 Smeared crack approach

There are several common methods of modeling RC cracks in FE applications. The two most common methods are discrete and smeared crack approaches. In discrete crack approach, a crack is first initiated at a certain location in the RC component. The growth in crack is determined by the nodal force at the tip of the crack exceeding a preselected tensile strength criterion. This process is continued when upon the increase in the demand and the violation of tensile strength criterion, the crack further splits into the nodes ahead of the existing nodes (de Borst et al. 2004). This requires constant remeshing when a crack grows into further nodes. Hence, the connectivity between nodes is constantly altered and the crack does not follow a path along the edge of

elements (Rots 1991). Due to the constant remeshing, such method of crack modeling requires time consuming analyses (de Borst et al. 2004).

In contrast to discrete crack approach, the reinforcing bars and cracks are assumed distributed over each element in smeared crack approach. The total stress carried by a RC component is equal to the summation of the averaged stresses in the cracked concrete and reinforcement. The averaged concrete stresses include parallel and normal stresses to cracks and the shear stress along the cracks. The averaged reinforcement stresses, by the rule of equilibrium, are determined based on the strains developed in the cracked element. The smeared crack approach is employed in two methods of fixed and rotating crack approaches. In the fixed crack approach, the cracks are fixed geometrically once they are generated. The normal and shear stress transfers are modeled separately and the principle stress vector does not necessarily coincide with that of the principle strain. Due to having the fixed direction of cracks, the prediction of cracking in a RC component by this method is relatively closer to reality (Maekawa et al. 2003). Conversely, as the name of the approach connotes, the main assumption of the rotating crack approach is that the directions of cracks coincide with the direction of principle strains. In other words, the cracks in an element rotate with the direction of the principle stress. In each step of computation, new cracks form in the element based on the stress condition and the previous cracks are erased from the memory (Maekawa et al. 2003).

The rotating crack approach assumes concrete as an orthotropic material and does not require separate hysteretic models for normal and shear stress responses of concrete (Vecchio 1999). The well-known models based on the concept of rotating crack approach are the Modified Compression Field Theory (MCFT) (Vecchio and Collins 1986) and the Disturbed Stress Field

Model (DSFM) (Vecchio 2000). The MCFT determines the load-deformation response of reinforced concrete membrane elements subjected to shear and normal stresses. Through the MCFT, one can calculate the average and local stresses and strains of concrete and reinforcement along with the width and orientation of cracks in elements. The MCFT is based on three sets of relationships. Assuming an orthogonally reinforced membrane element in *x*-*y* plane, the relationships include: compatibility relationships by which the average strains in concrete and reinforcement are assumed equal; equilibrium relationships by which the total normal stresses in both *x* and *y* directions equal to the summation of stresses in concrete and reinforcement and the shear stress totally carried by concrete; and the constitutive relationships for cracked concrete and reinforcement, relating the strains in compatibility relationships to stresses in equilibrium relationships (Vecchio and Collins 1986). The last assumption associates a single stress value to any strain value. Hence, MCFT is not directly applicable to cyclic loading. In addition, to account for the possibility of local yielding of reinforcement at a crack or sliding shear failure along a crack, MCFT limits the stresses at the crack and the average concrete tensile stresses (Wong and Vecchio 2002). This requires a shear crack check in the analysis.

To address the above limitations, DSFM was developed as a refinement of the MCFT. It eliminates the crack shear check in the MCFT through explicit calculation of crack shear slip deformations. In addition, it is developed as a secant stiffness-based model in order to be applicable to cyclic loading. Cyclic analysis produces plastic offsets strains in concrete and reinforcement. Hence, the model allows for pre-strain forces to be generated during when cyclic demand is applied (Vecchio 1999). The computation in the program is based on total-load iterative approach and setting a desired level of convergence criteria. The detailed description of

the non-linear FE algorithm used in VecTor2 program is provided in the work conducted by Wong and Vecchio (2002).

4.4.2 Analytical modeling of walls

The steps followed in the modeling of walls include defining the geometry of the walls and meshing of the geometry, applying the required constraints and the selection of the material properties and material constitutive models. These steps are described below.

Meshing

The walls in this study are modeled as full scale cantilever walls. Separate zones are required for modeling each wall due to variations in the ratio of flexural reinforcement provided in the web and boundary regions in addition to the separate top and bottom blocks. The top block is used for the application of the lateral loading in order to avoid crack concentration at the top of the walls and the bottom block restrains the wall at the end. It should be understood from earlier that the thickness is constant throughout the wall length due to being rectangular in cross section. In addition, the same concrete and reinforcement material properties are used for both boundary and web regions. The three distinct zones are shown in Figure 4.2.

Upon defining the required zones, discritization is performed. Meshing sizes selected herein are important in the final results where crack lengths for given crack widths are intended. In other words, overestimation of crack length might be obtained if element sizes smaller than required are selected and vice versa. In this study, the vertical sizes of elements-parallel to wall height- are selected as the expected vertical crack spacings in walls calculated by Eq. (38). This is to

enforce accurate spacing is provided between two consecutive cracks. In other words, constant spacing of cracks is assumed throughout the analysis.

$$s = 2c + \frac{s_b}{5} + \frac{k_1 k_2 d_b}{\rho_{ef}} \qquad \text{Eq. (38)}$$

In the above equation, c is the clear cover to the reinforcing bars, s_b is the spacing to the reinforcing bars, k_1 is a coefficient equal to 0.4 and 0.8 for deformed and plain bars, respectively. ρ_{ef} is the percentage of steel in the effective area of concrete and d_b is the diameter of the bars. k_2 is found from Eq. (39) in which ε_1 and ε_2 are the maximum and minimum tensile strains in the effective area of concrete respectively:

$$k_2 = 0.25\frac{\epsilon_1+\epsilon_2}{2\epsilon_1}, \begin{cases} \epsilon_1 = Max.Tension\ Strain\ in\ A_{c_{eff}} \\ \epsilon_2 = Min.Tension\ Strain\ in\ A_{c_{eff}} \end{cases} \qquad \text{Eq. (39)}$$

It is understood that initially spacing between cracks is high and reduces with increase in demand. Nevertheless, studies by Adebar and Van Leeuwen (1999) on large concrete beams indicate that the stabilization of crack spacing soon occurs in the response (at longitudinal strain approximately equal to 0.5mm/m). Thus, the initial linear reduction of crack spacing is not included in this study.

Meshing of the top and bottom blocks is selected in order to provide continuity with the wall. In essence, the horizontal element sizes are set equal to those in the web and boundary regions of the wall while the vertical sizes are selected in order to provide an appropriate aspect ratio for elements. The nodes at the bottom of the end slab are constrained in translation and rotation, providing fixity of the slab. Figure 4.2 shows the FE model of a typical wall in VecTor2 program. The three colours represent the distinct zones. Larger element sizes are used for second

half of the wall height. This is because in post-peak response of flexural shear walls, large repairable cracks are concentrated at the base of the wall and mainly in the plastic hinge zone. As such, larger elements used facilitate faster analysis without affecting the results.

Figure 4.2 FE model of RC shear wall

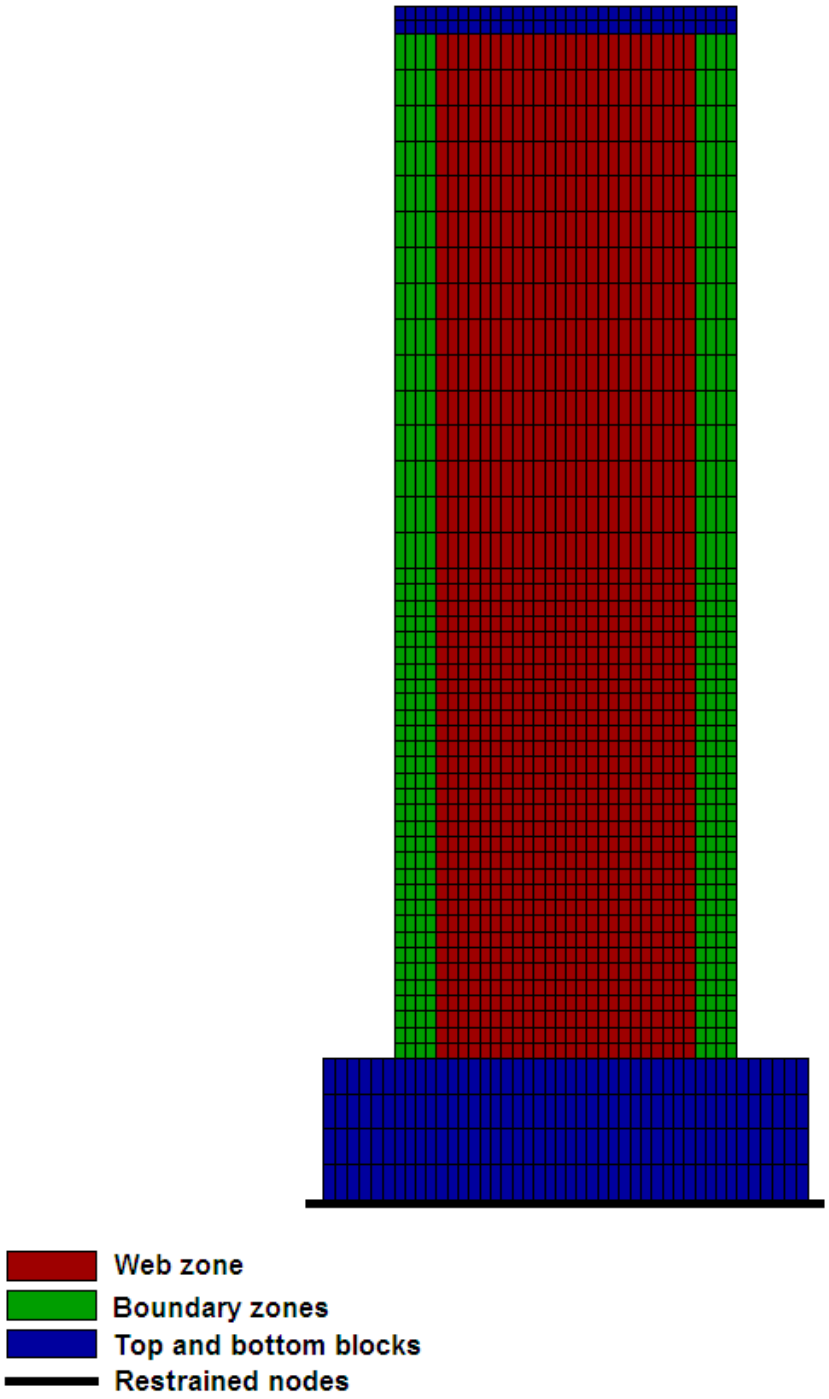

Selection of constitutive models

The VecTor2 program allows the selection of various material constitutive models depending on the type of analysis in hand. Considering the significant effect of constitutive models on the response of shear walls, a parametric study is conducted herein. The aim of such study is to assist in selection of the most appropriate material models. The parametric study includes the calibration of the behaviour of walls in terms of load-deformation responses from experimental results of selected tests in the literature with the predictions of VecTor2 program. The slender RC shear wall tested by Adebar et al. (2007) and the rectangular wall, RW1, tested by Thomsen IV and Wallace (1995) are selected for this purpose. The former was a large-scale wall of slenderness ratio 7 while the latter was a ¼ scale wall of slenderness ratio 3. The properties of both walls are provided in Table 4.3. Both walls were tested under constant axial loading of $0.1f'_cA_g$, in which f'_c is the concrete compressive strength and A_g is the gross cross sectional area. The reverse-cyclic lateral loading was also applied at the top of the walls.

Table 4.3 Properties of wall

Wall	Concrete Strength (MPa)	Reinforcement					
		(flexural)		(horizontal)		Yield Strength	Ultimate Strength
		Boundary	Web	Boundary	Web		
Tested by Adebar et al. (2007)	49	5-10M	10M at 305mm	No.3 at 64mm in the lower 3m	10M at 305mm	455MPa	650MPa
RW1 Tested by Thomsen and Wallace (1995)	31.6	8-9.5mm	6.35mm at 191mm	4.76mm at 51mm	6.35mm at 191mm	414MPa	480MPa-600MPa

The walls were modeled following the steps described earlier in the "Analytical modeling of walls". The average crack spacing in the wall tested by Adebar et al. (2007) is recorded as 240mm. The same value is used for discritization of the wall model. Although this spacing increased in the web region due to the lower amount of flexural reinforcement provided, constant spacing is assumed in the analytical model of the wall to avoid complexity of the mesh refinement. Due to lack of information on the average crack spacing in wall RW1, the refinement scheme proposed by Palermo and Vecchio (2007) is implemented. In this scheme, 14-16 elements are suggested to be used along the length of the wall. The aspect ratio to be used for the size of the elements is recommended to be less 1.5. The wall RW1 is modeled by 14 elements in the short direction with aspect ratio of 1.2. The envelope of the cyclic responses of the walls recorded during the tests are compared against the predicted responses from VecTor2 obtained using various constitutive models. Perfect bond is assumed between concrete and reinforcement.

The result of the study indicated that for the walls considered, Popovics models (Popovics 1973) for concrete compression pre-peak response and modified Park-Kent model (Park et al. 1982) for concrete compression post-peak response best capture the shape of the actual response curve. The wall tested by Adebar et al. (2007) is modeled by Popovics high-strength model and RW1 is modeled by Popovics normal-strength model. To model the reduction in stiffness and strength of concrete as a result of tensile straining, the Vecchio's 1992-A model (Vecchio and Collins 1993) is selected in which both the compressive strength and the corresponding strain are softened. Tension stiffening which is the effect of tensile stresses developed in concrete between the cracks due to the bond action between concrete and reinforcement is taken into account by Collins-Mitchell 1987 (Collins and Mitchell 1987) model. This model is found to match the response relatively better than the rest of the models though the differences among the results are

small. The remaining material models of concrete were selected as the default models in the program except for the hysteresis response of concrete (Palermo and Vecchio 2007). For the effect of tensile stresses developed in concrete as a result of post cracking, a linear descending tension softening model is used. The Kupfer model (Kupfer and Gerstle 1973) is used for the dilation of concrete representing the lateral expansion of concrete as a result of increase in compressive stresses. This effect leads to the presence of out-of-plain stresses for which the associated reinforcement in the third dimension is specified to provide the required confinement. The resulting increase in strength of concrete in compression is modeled by Kupfer-Richart model (Vecchio 1992). In the VecTor2 program, attention is also given to the width of cracks developed in concrete. By default, the compressive stresses are reduced when crack widths exceed 20% of aggregate size. The hysteresis response of concrete is modeled by the non-linear with cyclic decay model proposed by Palermo and Vecchio (2002). This model provides improvements such as accounting for nonlinear unloading and strength and stiffness degradation of reloading responses to the work conducted by Vecchio (1999). More importantly, it accounts for crack closure effects by using the model suggested by Okamura and Maekawa (1991). Seckin's model (Seckin 1981), accounting for strain hardening and the Bauschinger effect, is also used for the hysteresis response of reinforcement. The dowel action representing the shear resistance provided by reinforcement at the crack is not considered in the analysis.

The experimental and analytical responses obtained by VecTor2 using the models above for the wall tested by Adebar et al. (2007) are shown in Figure 4.3. The actual response of the wall prior the last cycle includes small residual displacements when the lateral force is decreased to zero. This is fairly well predicted by the analytical model of the wall. The predicted initial stiffness of the wall, the loading curves and the envelope of the response up to wall displacement of 180mm

are also close to the actual response. The minor variations of the analytical results occur in the last cycle at 2.4% drift ratio. The significant degradation of response in the last cycle is due to loss of concrete and fracture of flexural reinforcement. This is not captured by the analytical results due to no consideration of bar buckling effect. Hence, the large residual displacement of the wall in the last cycle when pushed to the east is not also predicted by VecTor2. It should be noted that this is not a concern for this study given the focus on pre-peak damage states.

Figure 4.3 Experimental and VecTor2 responses of wall tested by (Adebar et al. 2007)

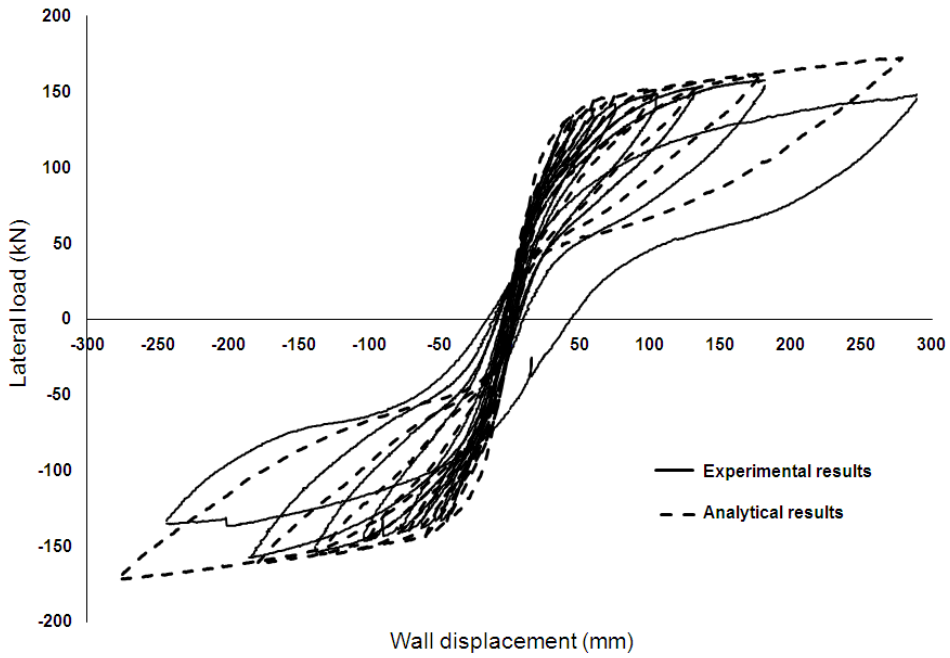

The experimental and predicted responses of RW1 by VecTor 2 and using the above constitutive material models are shown in Figure 4.4. The shapes of the loading and unloading curves of the response are in good agreement with the experimental results. Special attention is given to the residual displacements of the wall since these correspond to the occurrance of residual cracks.

The initial residual displacements and the maximum strength of the wall are also close to experimental observations. The predicted residual displacements the last four cycles, however, are under-estimated. During the test, the wall completed two cycles to the final amplitude before failure. The analytical results, however, show web crushing during the first cycle of the final displacement level. It should be again noted that the final damage stage is not the focus of this study.

Figure 4.4 Experimental and analytical responses of RW1

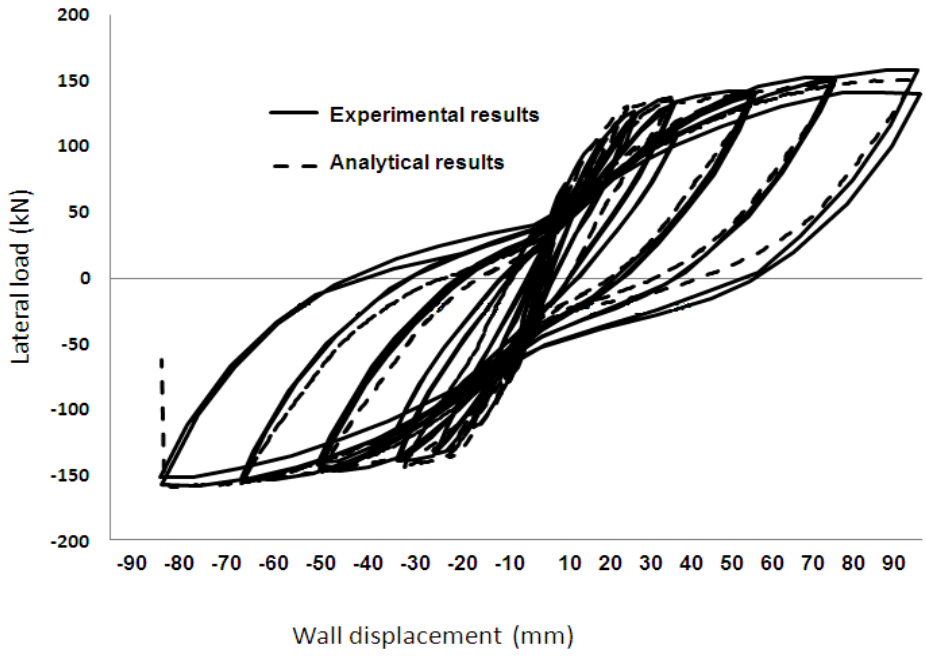

Comparisons of predicted and observed results of both walls are shown in Table 4.4 in terms of maximum lateral load and the corresponding maximum displacement. In general, the selected constitutive models provide satisfactory results. Although the above discussions reveal slight variations in the predicted results of both walls towards the end of response, the initial behaviour of walls are in good agreement with observations.

Table 4.4 Comparison of experimental and analytical behaviour of walls

Wall	Maximum Lateral Load (kN)			Corresponding Lateral Displacement (mm)		
	Analytical	Experiment	Ana./expt.	Analytical	Experiment	Ana./expt.
Tested by Adebar et al. (2007)	172.3	162	1.06	278.6	281.2	0.99
RW1 Tested by Thomsen and Wallace (1995)	158.3	158.23	1.00	77.15	80.46	0.95

4.5 Evaluation of damage predictions by VecTor2 program

The objective of this section is to evaluate the accuracy in the prediction of crack patterns including crack width and orientation by VecTor2 program. For this purpose, the results of the test conducted by Adebar et al. (2007) on the large-scale RC shear wall are used. This wall is selected for two major reasons. First, it is among very few large-scale walls tested in the literature. In addition, the test conducted by Adebar et al. (2007) is among the rare tests during which detailed measurements of cracks at various levels of demand are recorded. Photograph of crack patterns are also available taken at specific displacement levels.

The recorded data during the test include observed maximum crack widths corresponding to maximum deformation at each amplitude level. Hence, at the same level of displacements, maximum crack widths predicted by VecTor2 program are recorded for comparison. In the following, observed and predicted crack patterns and crack widths are compared separately.

Crack patterns

The observed and predicted crack patterns (including the extent and orientation of cracks) are compared for the final load stage due to the clarity of cracks traced from the photographs taken during the experiment. The observed crack pattern at specific points along the lower 3.6m of the wall is shown in Figure 4.5 for the final load stage. West and east are the negative and positive displacement directions, respectively. In this wall, a construction joint was designed at about 426mm above the base block, labelled C in the figure.

The crack pattern is not perfectly symmetrical in part because the wall was always displaced first to the east and then to the west during the test. The first horizontal flexural cracks occurred at the

construction joint of the wall. Along with increase in the displacement of the wall, new cracks formed at the locations of A, B and D. These cracks were also horizontal expect for the location D, at which the cracks were somewhat inclined. The next cracks to form were the inclined cracks at the locations I and J on the west side, and the horizontal cracks, F and G, on the east side. The vertical cracks at the very lower portion of the wall did not occur until the wall was displaced by ±200mm (about 1.7% drift ratio). This can be attributed to the reduction in strength of the wall, causing the compressive stresses to result in vertical cracks. The average spacing of the flexural cracks in the flanges was about 240mm.

The predicted crack patterns for the east and west sides of the wall are shown in Figure 4.6. As noted earlier, each element in the analytical model of the wall is 240mm in height. Hence, the locations of the predicted cracks along the height of the wall approximately correspond to those observed during the experiment. This leads to a comparable scale to be used for cracks on actual and analytical models of the wall. It should also be noted that the length of the wall below the construction joint is not modeled analytically. Hence, the 2880mm length shown in Figure 4.5 refers to the remaining height of the wall. The cracks with width larger than 0.1mm are shown with thick lines. Figure 4.6 shows the damage predicted on the west and east faces of the wall separately. This is because the images are taken from VecTor2 program when the wall is first pushed to the maximum east displacement and then to the maximum west displacement.

Comparison of the observed and analytical results shows that the horizontal cracks at the boundary regions of the wall are well predicted. Generally, the patterns of the inclined cracks at the web region are similar to the observed results. The small elevation difference between the

construction joint and the base block is not accounted for in the analytical modeling. As such, the largest analytical cracks occur at the joint location of the wall to the base block.

Figure 4.5 Observations of crack pattern at final load stage (Adebar et al. 2007)

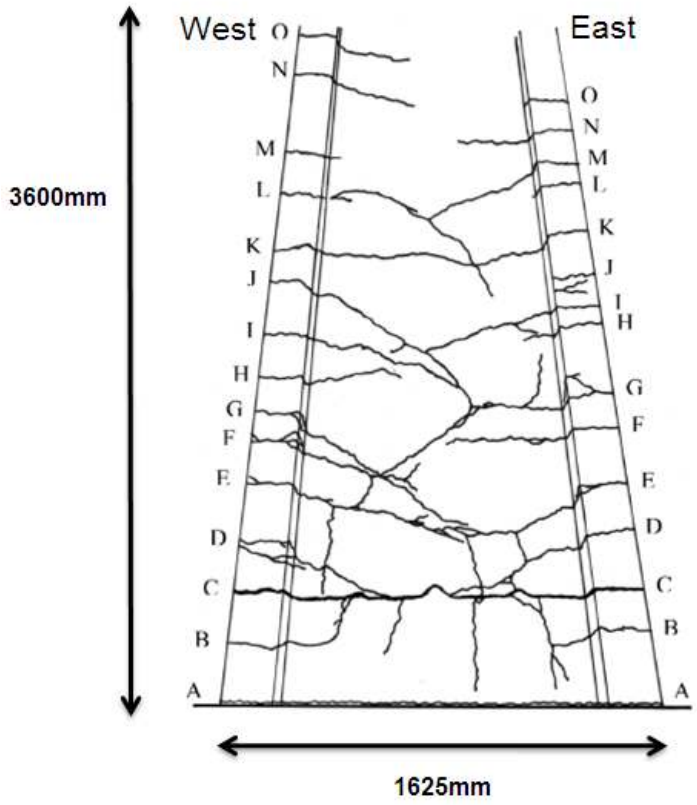

Figure 4.6 Predicted crack pattern at final load stage: a) west face; b) east face

(a)

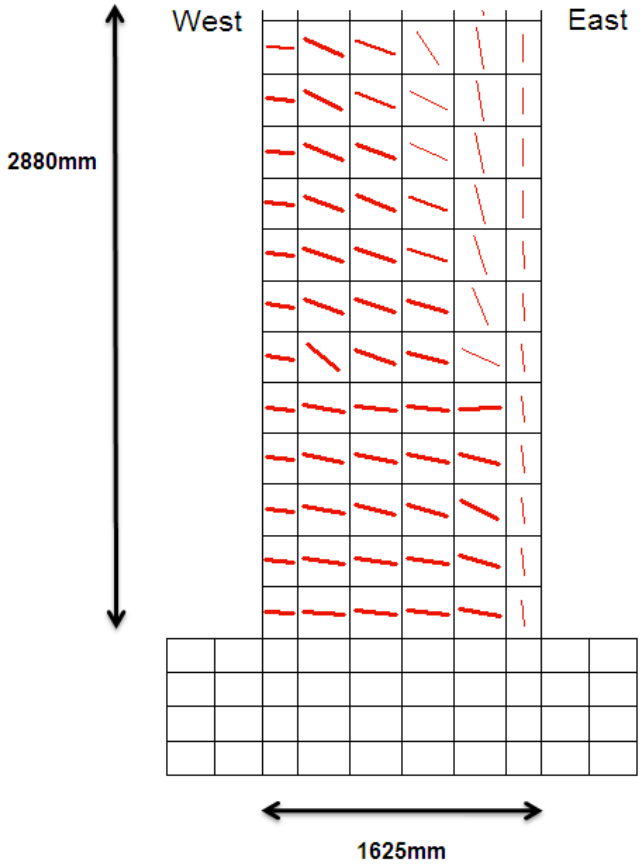

(b)

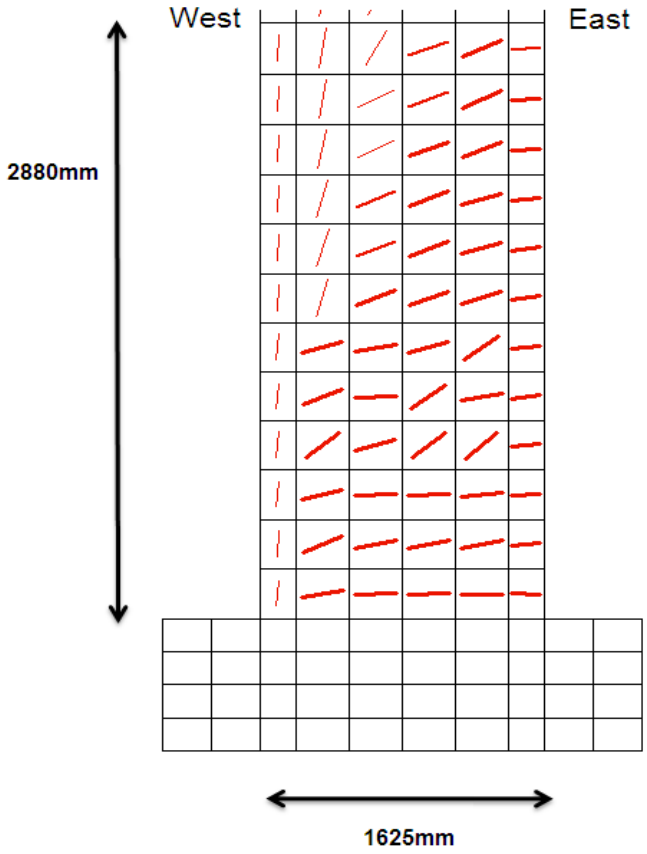

Crack widths

The observed and analytical crack widths for the lower 2.5m (approximately) of the wall height observed at various wall displacements are compared in Table 4.5. The maximum crack width occurs at the location of the construction joint during the experiment, labelled C. This location corresponds to the base of the analytical wall also labelled C. For the actual wall, the width of cracks at locations A and B below the construction joint never became wider than 0.3mm due to the additional flexural reinforcement provided.

The reduction in crack width with increase in the elevation of the wall is captured by VecTor2. The difference, though, lies is in the predicted values of crack width. In the actual results, the cracks on the east face are almost twice those of the west face for locations C and D when the wall is displaced beyond ±105mm. This unsymmetrical damage is not predicted by VecTor2. The analytical crack widths are closer to those of the east face except for the wall displacement of -187mm. The ratios of observed versus analytical results for the east face of the wall are shown are Table 4.6 in addition to the means and standard deviations of the ratios for each displacement level. Except for displacement at -104mm, the mean of the ratios are close to 1. Nevertheless, no general conclusion on the accuracy of crack width prediction by VecTor2 program can be made. Indeed, the above comparison is made considering only the results of one wall. More accurate conclusions could be gained if the results of additional walls were considered. It should also be noted that the aim of the probabilistic model developed in this study is not solely in the accuracy of prediction. The model development process and the insight gained on the significance of the design variables on cracking in walls are also among the objectives of the developed model herein.

Table 4.5 Comparison of maximum crack width: a) observed and b) predicted

a)

West Face (Measured)	**Wall Displacement (mm)**				
	46	**74**	**105**	**132**	**182**
J	0.3	0.3	0.3	0.3	0.3
I	0.15	0.2	0.4	0.4	1
H	-	-	0.25	0.3	0.4
G	-	-	0.25	0.5	1.25
F	-	0.35	0.5	1.25	1.5
E	-	0.5	1.0	2.0	3
D	0.5	0.8	1.25	1.5	3
D	-	-	0.5	1.5	1.5
C	0.8	1.25	1.5	0.3	4
B	0.1	0.2	0.2	0.3	0.3
A	0.15	0.2	0.25	0.3	0.3
East Face (Measured)	**Wall Displacement (mm)**				
	-49	**-77**	**-104**	**-138**	**-187**
I	-	-	-	0.6	0.3
H	-	0.1	0.25	0.4	0.4
G	0.3	0.5	0.4	0.6	0.8
F	0.15	0.4	0.4	1.0	1.2
E	-	0.6	0.5	1.0	1.5
D	0.25	0.6	0.8	1.25	3
C	0.8	1.5	3	3.5	7
B	0.1	0.15	0.1	0.15	0.25
A	0.15	0.2	0.25	0.3	0.3

b)

West Face (Analytical)	Wall Displacement (mm)				
	45	**75**	**104**	**134**	**193**
I	0.11	0.31	0.38	0.38	0.45
H	0.20	0.38	0.43	0.43	0.5
G	0.23	0.44	0.48	0.47	0.54
F	0.25	0.46	0.49	0.5	0.96
E	0.29	0.49	0.62	1.7	2.53
D	0.32	0.64	1.87	3.13	3.32
C	0.42	1.6	2.81	3.1	3.63
East Face (Analytical)	Wall Displacement (mm)				
	-45	**-75**	**-105**	**-134**	**-179.1**
I	0.11	0.31	0.39	0.49	0.55
H	0.19	0.38	0.43	0.45	0.52
G	0.22	0.43	0.47	0.49	0.62
F	0.26	0.47	0.5	0.86	0.91
E	0.32	0.49	0.61	1.73	2.55
D	0.35	0.5	2.27	3.1	3.36
C	0.37	1.83	2.59	3.04	3.47

Table 4.6 Ratio of observed to predicted crack width (east face)

West Face (East)	Wall Displacement (mm)				
	-49	**-77**	**-104**	**-138**	**-187**
I	-	-	-	1.22	0.54
H	-	0.26	0.58	0.89	0.77
G	1.36	1.16	0.85	1.22	1.29
F	0.58	0.85	0.80	1.16	1.31
E	-	1.22	0.82	0.58	0.59
D	0.714	1.2	0.35	0.40	0.89
C	2.16	0.82	1.15	1.15	2.02
Mean	1.2	0.91	0.75	0.94	1.05
Standard deviation	0.72	0.36	0.27	0.33	0.52

Some concrete cover spalling was observed on the compression face of the wall during the test at about 180mm of wall displacement, prior reaching post-peak response. Concrete cover spalling is not, however, predicted by the analysis. This is due to modeling the cover concrete as confined concrete (the boundary zones are entirely modeled with membrane elements confined with reinforcement in both directions). Indeed, this affects the computation of predicted crack length. The minor spalling which might occur in walls prior peak response essentially would be predicted as cracks in membrane elements, slightly over-estimating the total length of cracks.

4.6 Analysis of walls

The earlier sections of this chapter discussed the list of walls to be used for the development of the database of expected cracks. The sections also demonstrated the analytical modeling of walls in addition to evaluating the accuracy of predictions by VecTor2 program in terms of crack patterns and width. The next step is to select the loading history to be applied on walls for the non-linear cyclic analysis. This is presented below proceeded by the method of computation of crack length during the analyses.

Loading history

Except for wall NO.6 which carries no axial load (refer to Table 4.2), the constant axial load is applied as distributed axial load on the top slab. The reversed cyclic lateral load is applied on the side of the top slab, displacing the wall to both negative and positive directions. Special attention is given to the selection of the lateral loading history due to its effect on the response and performance of walls. The loading scheme including the axial and lateral loads applied on walls are shown in Figure 4.7.

Figure 4.7 Loading scheme

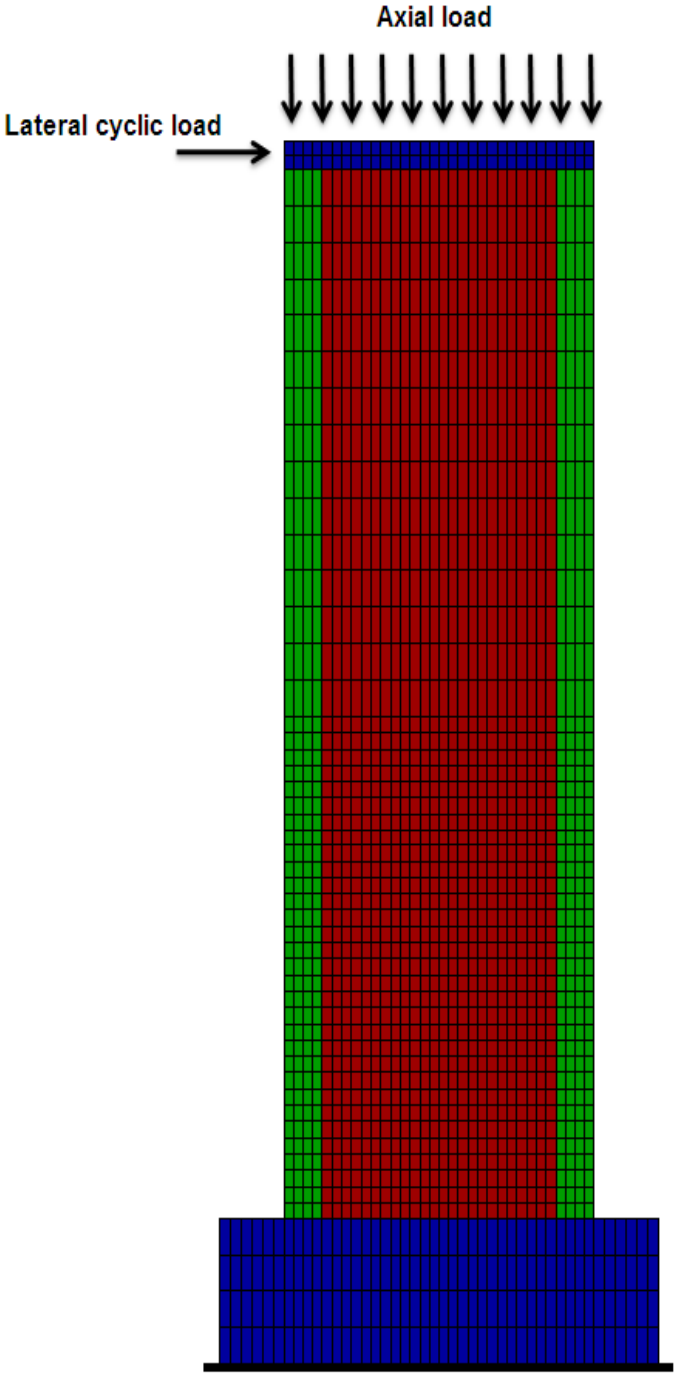

The selection of a loading history generally depends on two factors: identification of the intended damage states and the demand parameter which correlates with the targeted damage states (FEMA 461 2007). The damage state identified herein is the occurrance of cracks in RC shear walls which require epoxy injection. Preliminary studies on damage to walls conducted herein indicate that such cracks are mainly associated to the response of walls after yielding of flexural reinforcement. Hence, the intended damage state occurs with the onset of yielding of flexural reinforcement. Clearly the associated demand parameter after yielding of walls is the applied displacement demand. The selected load history is shown in Figure 4.8 and is based on studies on various loading histories used in literature. The details of this study are presented in Appendix B.

Figure 4.8 Selected loading history

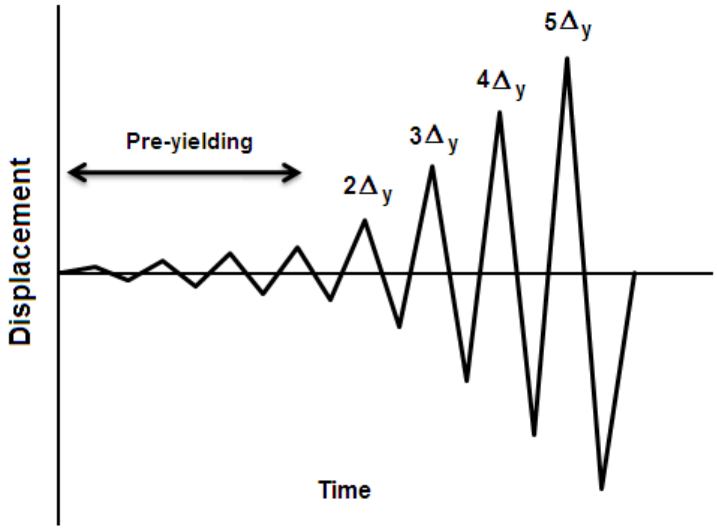

Computation of crack length

The computation of total crack length is described in this section. After completing of each cycle when the applied load returns to zero, the repairable residual cracks corresponding to the residual displacement of the wall are determined. As mentioned earlier, the residual crack widths are the required data for model development considering the ultimate purpose of the proposed methodology is the associated losses after occurrance of an earthquake. To measure the length of residual cracks a code in Matlab program was developed. The repairable cracks have widths larger than 0.5mm, as identified previously. For the walls considered herein, such cracks occur after yielding of flexural reinforcement. The widths of such cracks never exceeded 3mm during the analyses. The total crack length is determined as the summation of length for all elements with repairable cracks. As expected, analysis results indicate that most cracks are flexural (parallel to wall base). Considering the similar repair action used for shear and flexural cracks at early levels of damage, the two types of cracks are summed to determine the total crack length. Analyses conducted herein show the width of flexural and shear cracks do not exceed 6.5mm and 3mm, respectively. For such cracks, the application of epoxy injection is proposed by FEMA 308 (1998). The total crack length is then normalized by the length of walls and recorded as one observation paired with the level of demand and the associated design variables.

The above process is repeated for all the cycles used for analysis of each wall up to peak strength. Hence, the number of paired observations for each wall is equal to the number of cycles the wall undergoes up to peak response. The figure below further illustrates the variation of crack length as a function of demand for each design variable.

Figure 4.9 Variation of crack length for each design variable

a) Concrete compressive strength (f'_c)

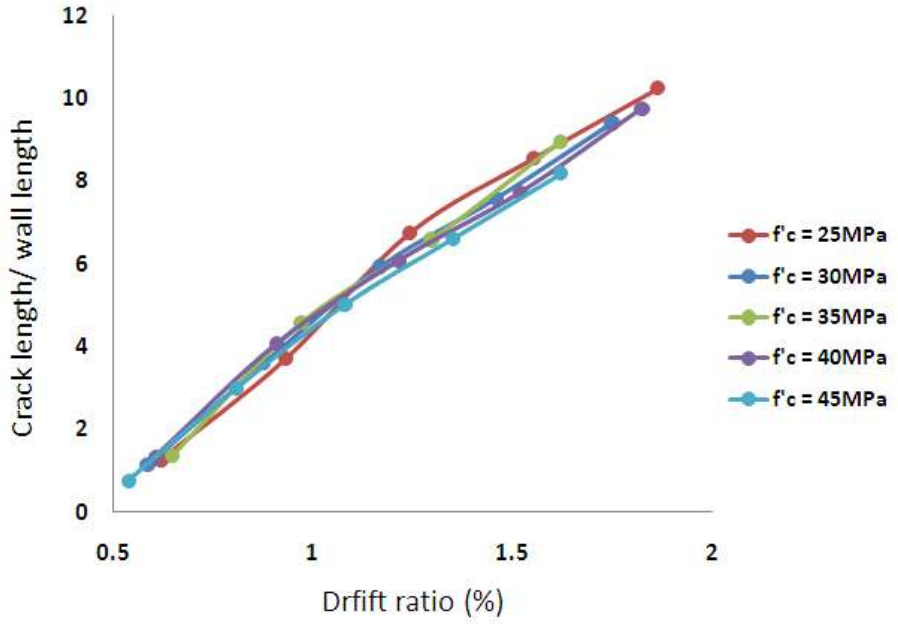

b) Axial load ratio (γ)

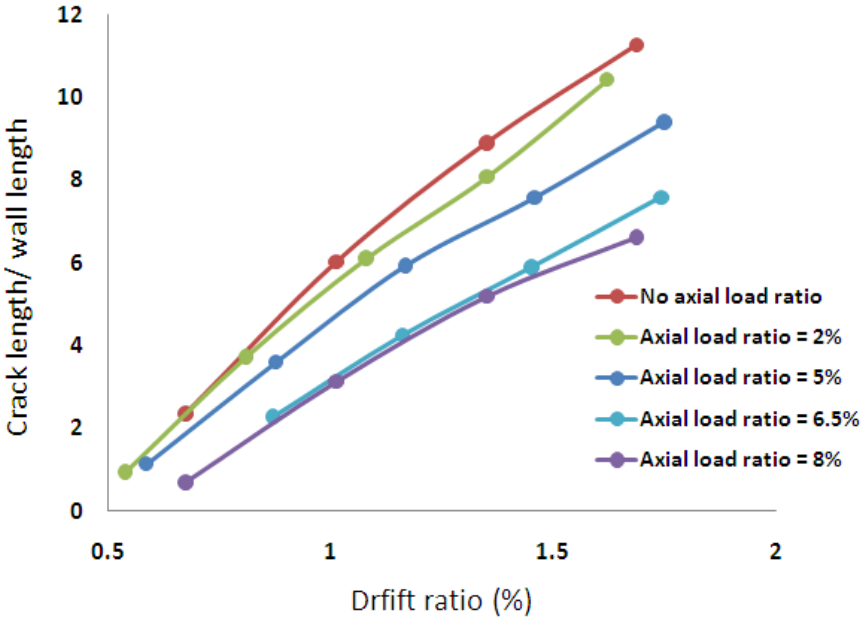

c) **Web flexural reinforcement ratio (ρ_{lw})**

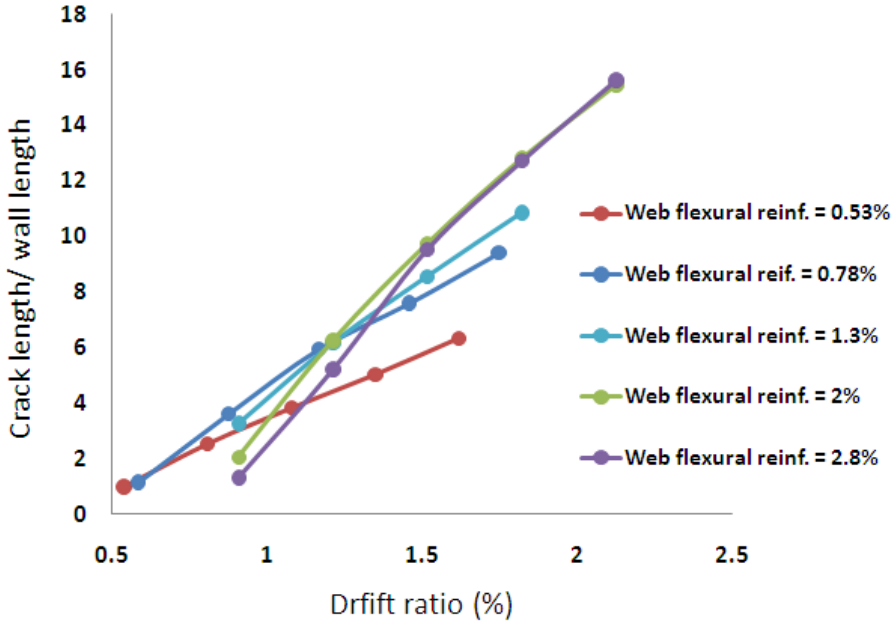

d) **Boundary flexural reinforcement ratio (ρ_{lb})**

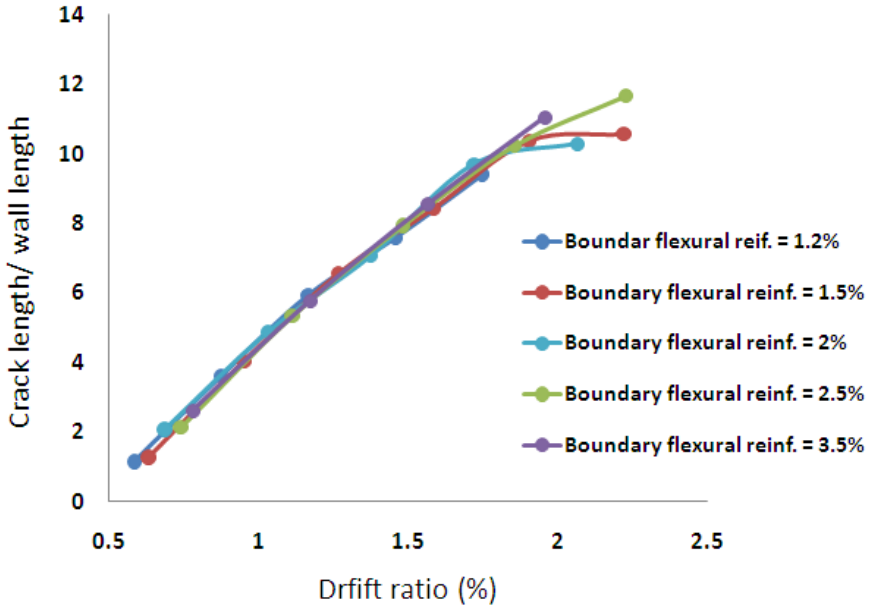

e) Horizontal reinforcement ratio (ρ_h)

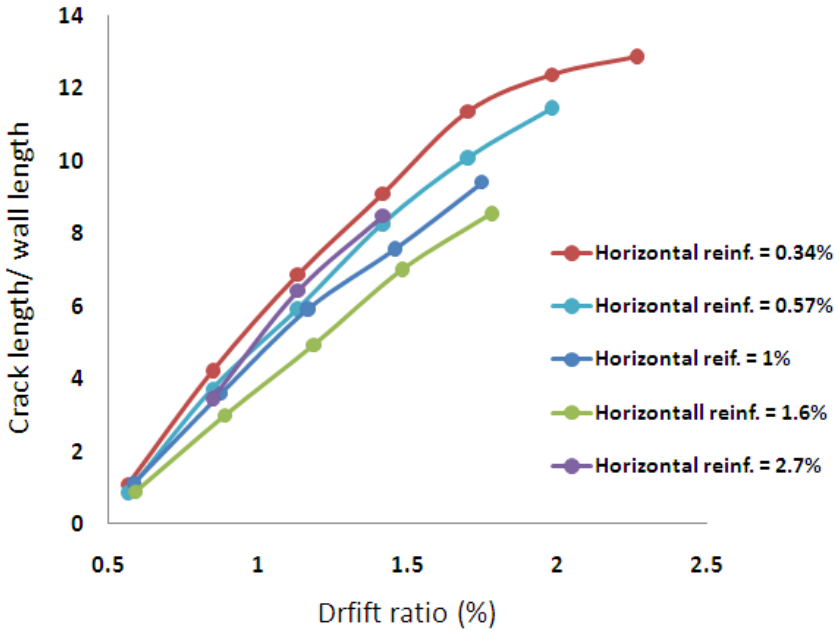

f) Horizontal reinforcement ratio (ρ_h)

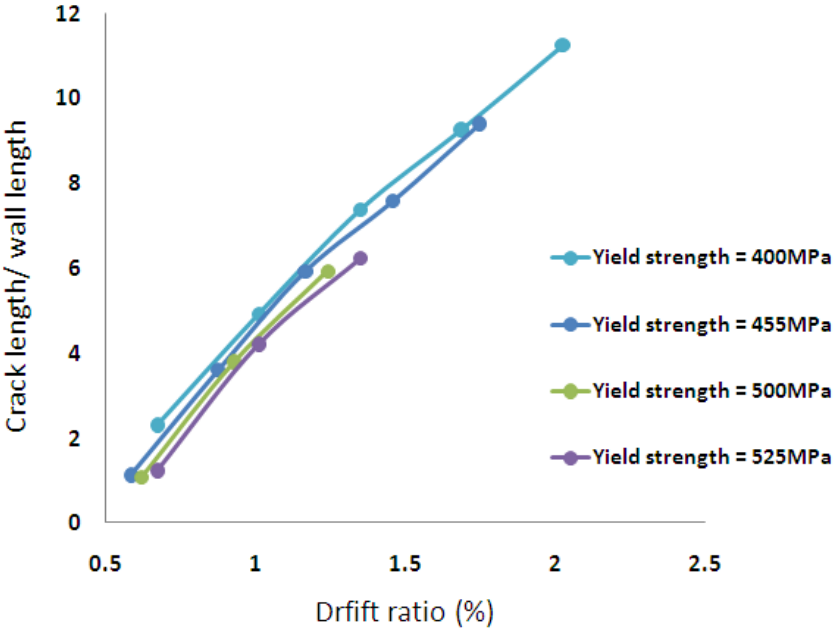

g) Slenderness ratio (h_w/l_w)

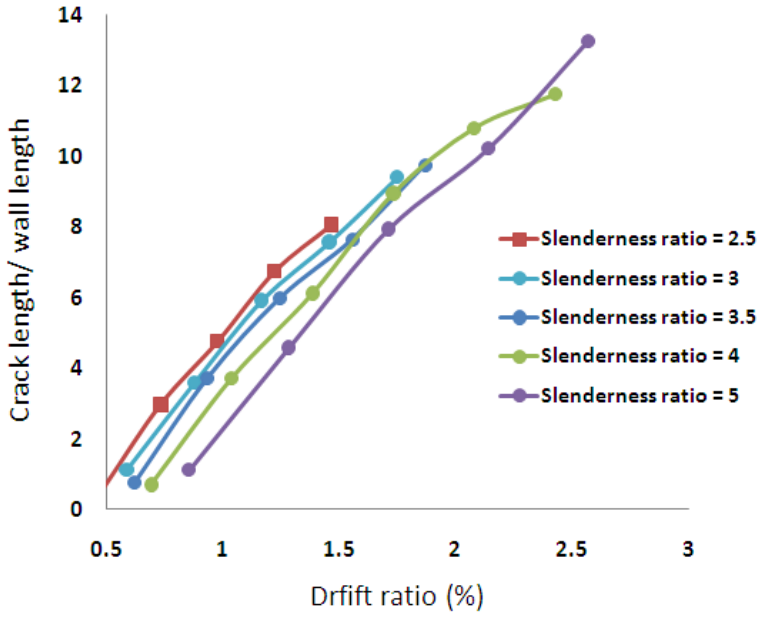

5 Probabilistic Model of Crack Length

5.1 Selection of explanatory functions

In Chapter 4, an example of data generation procedure for probabilistic model development was presented. This chapter utilizes the data to develop a continuous probabilistic model of crack length for RC shear walls. The intended linear probabilistic model of crack length is give by Eq. (40) in which measures of crack length are normalized by the length of walls to develop a dimensionless model:

$$\frac{l_{crack}}{l_w} = \theta_1 h_1(\mathbf{x}) + \theta_2 h_2(\mathbf{x}) + \cdots + \sigma\varepsilon \qquad \text{Eq. (40)}$$

l_{crack} is the total length of residual cracks corresponding to the applied displacement demand and l_{w} is the length of walls. The first step in model development is the selection of the explanatory functions on the right side of Eq. (40). For this purpose, each design variable listed in Table 4.2 is set equal to an explanatory function. In other words, multiple combination of design variables in defining an explanatory functions is avoided, though possible based on mechanics and engineering judgement. This is followed in part because the significance of each single design variable on damage to walls is sought. For brevity, these variables are repeated in Table 5.1. Except for the values of story drift, the remaining explanatory functions are constant while the crack length increases in each wall as a function of story drift. The reason for the inclusion of applied demand as a model variable is two-fold. It is first recognized that crack length is mainly a function of applied displacement demand. Second, to develop continuous a model, a variable whose value constantly changes along with crack length is needed. In essence, the values of design variables are constant for each wall and alone cannot capture the continuous change in the

values of crack length with changes in loading. The demand is in terms of maximum story drift, determined as the maximum displacement of the last completed cycle. Story drift is chosen to obtain dimensionless measures of demand. It should be reminded that, since no repairable crack is observed prior yielding of walls, the effect of force-controlled demand is not included in modeling of total crack length.

Following Eq. (40), the explanatory functions are linearly added. Clearly, such linear combination results in the θ parameters of concrete tensile and compressive strength and the yield strength of flexural reinforcement to have various dimensions while the rest of model parameters are dimensionless. It is possible to normalize these explanatory functions with appropriate coefficients, such as 100MPa for yield strength of flexural reinforcement. Nevertheless, this is not performed at this step herein.

Table 5.1 List of explanatory functions

Variables	Symbol	Explanatory Functions	Range
Drift ratio	δ	$h_1(x)$	Variable between walls
Concrete tensile strength	$\sqrt{f'_c}$	$h_2(x)$	5-6.71
Concrete compressive strength	f'_c	$h_3(x)$	25-45MPa
Axial load ratio	$P/A_g f'_c$	$h_4(x)$	0-8%
Flexural reinforcement (web)	ρ_{lw}	$h_5(x)$	0.54-2.8%
Flexural reinforcement (boundary)	ρ_{lb}	$h_6(x)$	1.2-3.5%
Horizontal reinforcement (web & boundary)	ρ_h	$h_7(x)$	0.34-2%
Yield strength of flexural reinforcement	f_y	$h_8(x)$	400-525MPa
Slenderness ratio	h_w/l_w	$h_9(x)$	2.5-5

5.2 Parameter estimation

Having defined the explanatory functions, the next step is to assess the model by estimating the statistics of model parameters, $\boldsymbol{\Theta} = (\theta_1, \theta_2, \ldots, \sigma)$. For this purpose, the closed-form algorithm described in Chapter 3 and proposed by (Gardoni 2002a) is followed. Due to lack of information on the prior distribution of θ values, the non-informative prior shown in Eq. (25) is used. As mentioned earlier, such prior distribution would not have significant effect on the posterior distribution of θ parameters due to the large number of observations collected. The model development process includes an iterative procedure between the application of the Bayesian inference to calculate $\boldsymbol{\Theta}$ and the deletion process (described at the end of Chapter 3). At each iteration, statistics of $\boldsymbol{\Theta}$ are first calculated by the closed-form algorithm written in a code using Matlab program (MathWorks 2009a). Then the explanatory functions whose θ parameters have large coefficient of variations, COV, are identified as insignificant. This is because the inclusion of such explanatory functions does not improve the model accuracy. Hence, the model becomes simpler in form simpler by removing them. Upon omission of such explanatory functions, the model is further assessed by recalculation of $\boldsymbol{\Theta}$ and identification of further insignificant explanatory functions. This is to achieve an optimization between model accuracy, in terms of a minimum value of model error, and model simplicity, in terms of as few explanatory functions as possible (Gardoni 2002a).

The summary of the deletion process is shown in Figure 5.1. In this figure, the COV of θ parameters (solid circles) are shown at each step along with the posterior mean of the model error (open squares). The explanatory function whose θ coefficient has the largest COV at each

step is indicated by a cross mark. The corresponding numbers of the omitted explanatory functions are shown adjacent to the cross marks.

Figure 5.1 Deletion process of model assessment

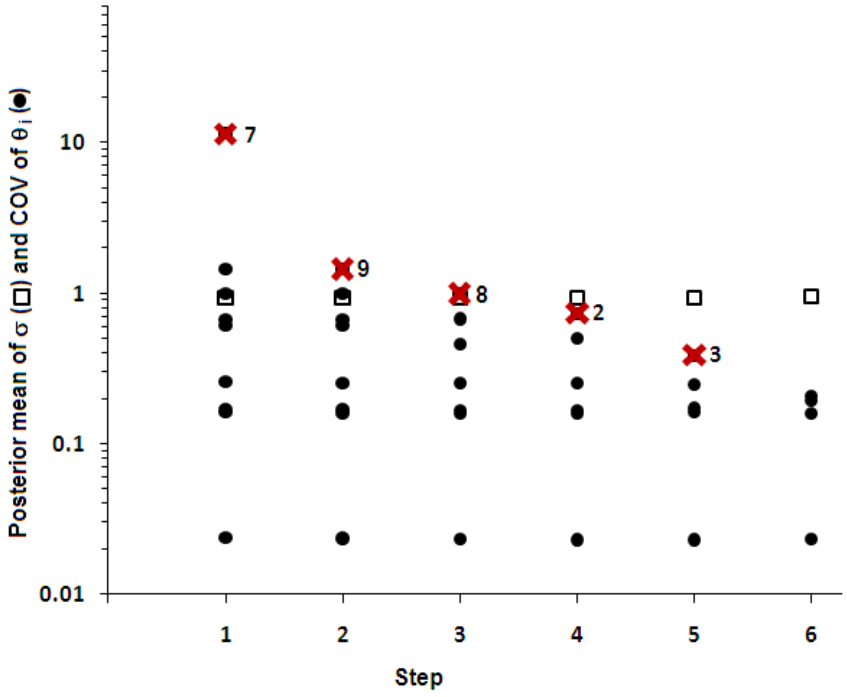

The first step includes all the nine explanatory functions linearly added in the model. Assessing the model results identifies the first insignificant explanatory function as the ratio of flexural reinforcement in the boundary region, ρ_{lb}, with COV equal to 11.42. The posterior mean of the model error is 0.93 in this step. The yield strength of reinforcement is identified as the most insignificant explanatory function next, with COV equal to 1.44. The model error has posterior mean of 0.92 in the second step. In the consecutive steps, the ratio of horizontal reinforcement is removed followed by the compressive and tensile strength of concrete. The simplest model for is achieved in the sixth step, after which any further reduction deteriorates the model. In the final

step, the posterior mean of the model error is 0.95 which an indication of no significant deterioration of the model. The final model is written as:

$$\frac{l_{crack}}{l_w} = \theta_1\delta + \theta_4\frac{h_w}{l_w} + \theta_5\frac{P}{f'_c A_g} + \theta_6\rho_{lw} + \sigma\varepsilon \qquad \text{Eq. (41)}$$

The remaining explanatory functions are all dimensionless leading to a dimensionless model. The significance of axial load ratio and the ratio of flexural reinforcement in the web is well understood. Axial load ratio reduces the tensile strains developed in concrete and vertical reinforcement as a result of seismic loading. Consequently, fewer cracks develop. Axial load ratio also increases the crack closure effect. After occurrance of cracks, the tensile strains are carried by the vertical reinforcement. Clearly, more cracks are expected to develop if low ratios of reinforcement are provided. As mentioned in Chapter 4, slenderness ratio indirectly affects the total length of cracks by increasing the number of cycles the wall undergoes, causing further damage. Among the insignificant explanatory functions is the ratio of flexural reinforcement in the boundary region of the wall. This parameter significantly controls the response as it has direct effect on strength and stiffness of shear wall. However, the boundary regions of the walls designed herein are relatively quite small in length compared to the length of the web regions. As such, variations in the length of cracks developed in these regions are not considerable in the total length of cracks calculated at each demand level. The yield strength of flexural reinforcement is also expected to have contribution to damage in walls. This parameter controls the response of shear walls subjected to seismic loads when significant tensile strains are produced and carried by the reinforcement. Nevertheless, the range of variations in the values of yield strength of reinforcement is considerably narrow in this study, taking into account the

limitations imposed by the design code. Hence, compared to other variables, changes in the value of this explanatory function are not significant compared to the effect of other variables.

Figure 5.2 shows the comparison of normalized crack lengths computed by VecTor2 program with the median values ($\varepsilon = 0$) of normalized crack length predicted by the probabilistic model. For a perfect model, the data would line up along the 1:1 solid line. The dotted lines delimit the region within ±1 standard deviation, indicating the lower and upper bounds, respectively. Except few data points, the majority of data fall within the bounds indicating low dispersion in predictions. The points with highest dispersion at low and high levels of crack length refer to the model predictions for walls with high ratios of flexural reinforcement in the web region. The model tends to overestimate total length of cracks at low levels of demand and otherwise.

The statistics of the model parameters are shown in Table 5.2. High correlation is observed between parameters θ_4 and θ_5. For $\rho_{ij} \geq 0.7$, Gardoni et al. (2002b) suggests combining the two model parameters following Eq. (31). This indicates that the model can be further simplified. Nevertheless, this is not performed at this stage since diagnostics are checked first. Diagnostics remedies further alter the statistics of the model parameters. This is discussed in the next section.

Figure 5.2 Comparison of computed to median predicted crack length

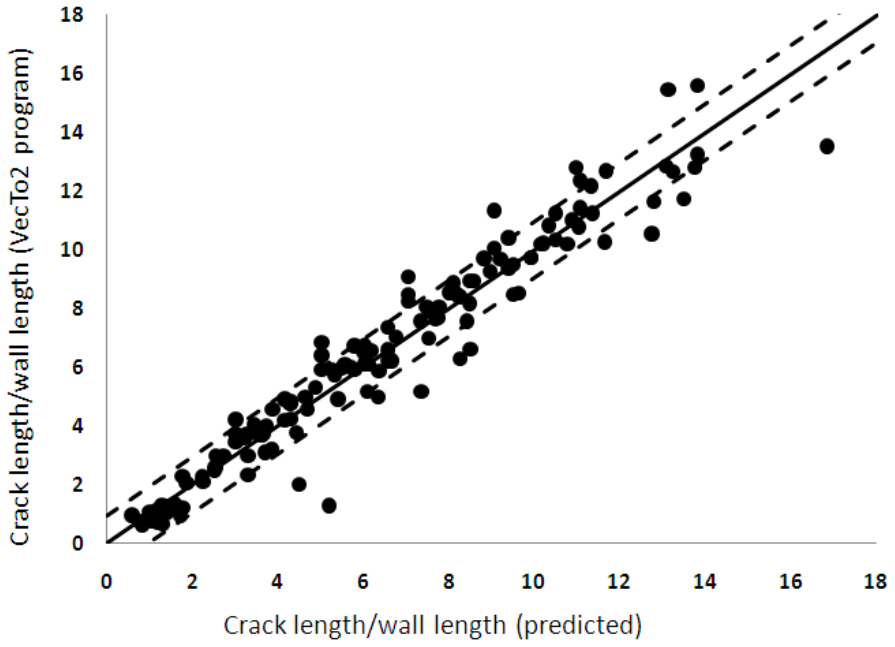

Table 5.2 Statistics of model parameters

Coefficients	Mean	COV	Correlation coefficient			
			θ_1	θ_4	θ_5	θ_6
θ_1	7.1	0.023	1.00	-0.52	-0.02	-0.16
θ_4	-0.72	0.16	-0.52	1.00	-0.70	-0.18
θ_5	-0.31	0.19	-0.02	-0.70	1.00	-0.20
θ_6	0.86	0.21	-0.16	-0.18	-0.20	1.00
σ	0.95	0.06	-	-	-	-

5.3 Diagnostics

As understood earlier, probabilistic model development is an iterative procedure between the application of Bayesian inference and diagnostics. This is important because there are some standard assumptions behind the least square theory which should be violated throughout model development process. Considering the Bayesian inference being based on the least square regression analysis, the same assumptions apply. Hence, assurance is required to justify such assumptions. Possible diagnostics including existence of outliers among the data, normality of errors and homoskedasticity are checked for in this section.

5.3.1 Outliers

Among the data used, outliers are the observations associated with extreme errors. The existence of such data affects model accuracy. In addition, the assumption of model errors distributed according to normal distribution (normality of errors) might be violated if errors are highly scattered. Normality of errors is one the standard assumptions behind least square regression and hence the application of Bayesian approach followed herein. To check for the possibility of outliers, the squares of model residuals are plotted against the model predictions in Figure 5.3. In this plot, some data points are associated with high residuals whereas the majority of data are gathered around the zero point on of the ordinate axis. Although this plot provides an insight on the distribution of the model errors, care should be taken when detecting the outliers. Visual inspection might not be always accurate as some data might be seen as largely deviated from the rest of data but not be statistically an outlier.

Figure 5.3 Model residuals against model predictions

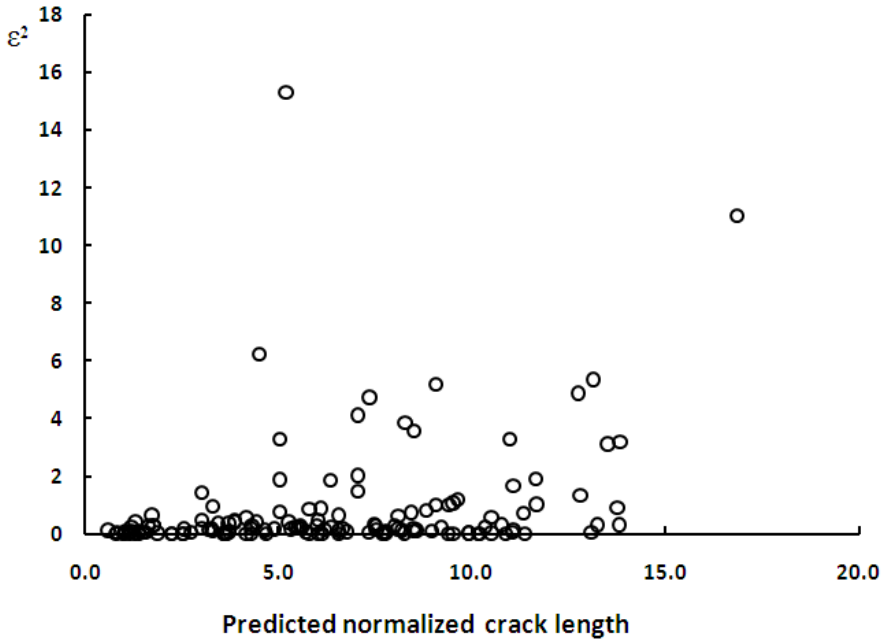

In this work, the detection of outliers is based on the *generalized extreme studentized deviate many-outlier procedure* proposed by Rosner (1983). In this methodology, l number of outliers is detected by first computing the extreme studentized deviates, R_i, from successively reduced sample of size n. R_i is given by:

$$R_i = \max_{i=1,\ldots,n} |\varepsilon_i - \bar{\varepsilon}|/s \qquad \text{Eq. (42)}$$

in which $\bar{\varepsilon}$ is the mean value of errors, $\boldsymbol{\varepsilon} = (\varepsilon_1, \ldots, \varepsilon_n)$ and s represents the stand deviation of errors. Assuming a criterion equal to α, representing the desired confidence level, λ_i is sought such that:

$$Pr\left\{\bigcap_{i=l+1}^{k} [(R_i \leq \lambda_i | H_l)]\right\} = 1 - \alpha \qquad \text{Eq. (43)}$$

where Pr indicates the probability that the hypothesis, H_l, that l number of outliers exists is true. Based on the studies conducted by Rosner (1983), $\alpha = 0.05$ for $n \geq 25$.

Following the approach described above, 14 outliers are detected for the sample of observations used herein. These outliers are shown in Figure 5.4 in red circles. They are mainly associated to the model predictions for walls NO. 13 and 14 with the highest ratios of web flexural reinforcement equal to 2% and 2.8%. Indeed, the same data points were also observed with high dispersion in Figure 5.2 lying below and above the ±1 SD bounds. These outliers are also summarized in Table 5.3.

Figure 5.4 Detection of outliers

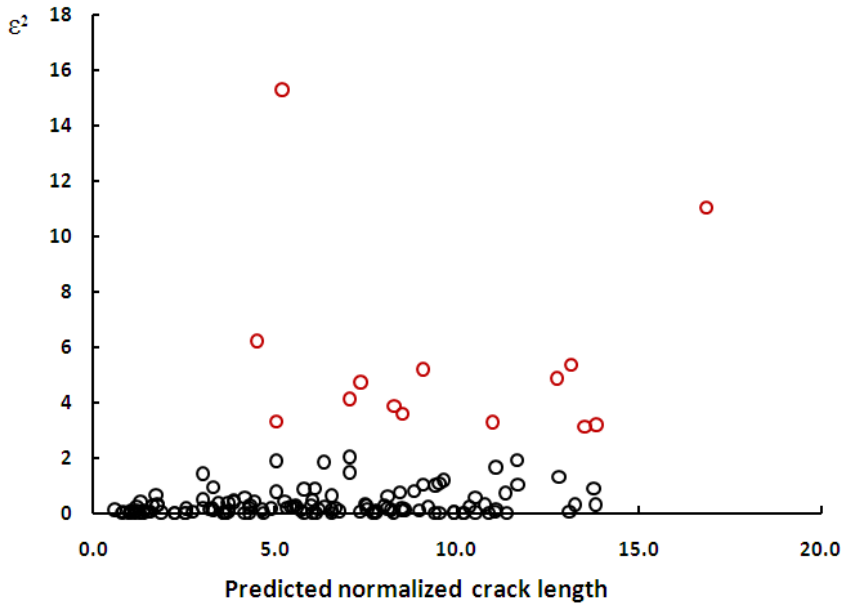

Table 5.3 List of outliers

Wall NO	l_{cr}/ l_{wall} (VecTor2)	l_{cr}/ l_{wall} (median prediction)	Square of residuals
10	6.30	8.27	3.86
12	6.22	4.50	2.94
12	12.79	10.97	3.29
12	15.45	13.13	5.36
13	1.29	5.19	15.28
13	5.18	7.35	4.71
13	15.61	13.82	3.20
14	10.54	12.74	4.84
18	6.85	5.03	3.31
18	9.07	7.04	4.12
18	11.33	9.05	5.20
27	11.74	13.50	3.10
28	13.52	16.84	11.02

Almost all outliers are associated to the extreme values of the design variables. In particular, wall NO 10 has the least ratio of web flexural reinforcement whereas walls NO 12-13 have the highest ratio. Also, wall NO 14 is associated with the largest ratio of flexural reinforcement in the boundary region, wall NO 14 with the least ratio of horizontal reinforcement and walls NO 27-28 have the highest slenderness ratios. Figure 5.5 shows the updated model after omitting the outliers. Clearly the model is improved by the removal of the majority of points lying outside of the bounds. The updated statistics of the model parameters are also shown in Tabl5 5.5. Notable is the reduction in the COV of θ_6, associated with web flexural reinforcement, form 21% to 14%. The model is slightly improved by the reduction in the posterior mean of the model error form 0.95 to 0.58. The mean of the ratio of computed crack length to median values of predicted crack length is still 0.99 but COV is slightly reduced to 0.158.

It should be mentioned that removing the outliers limits the applicability range of the model. This is because the ranges of design variables are further narrowed if the associated data points are removed when developing the probabilistic model. The applicability range of the updated model is as follows:

Table 5.4 Model applicability range

Design variable	f'_c **(MPa)**	γ	ρ_{lw}	ρ_{lb}	ρ_h	f_y **(MPa)**	h_w/l_w
Applicability range	25-45	0-8%	0.78-1.26%	1.20-3.5%	0.57-2%	455-500	2.5-3.5

Figure 5.5 Comparison of computed to median predicted crack length updated model

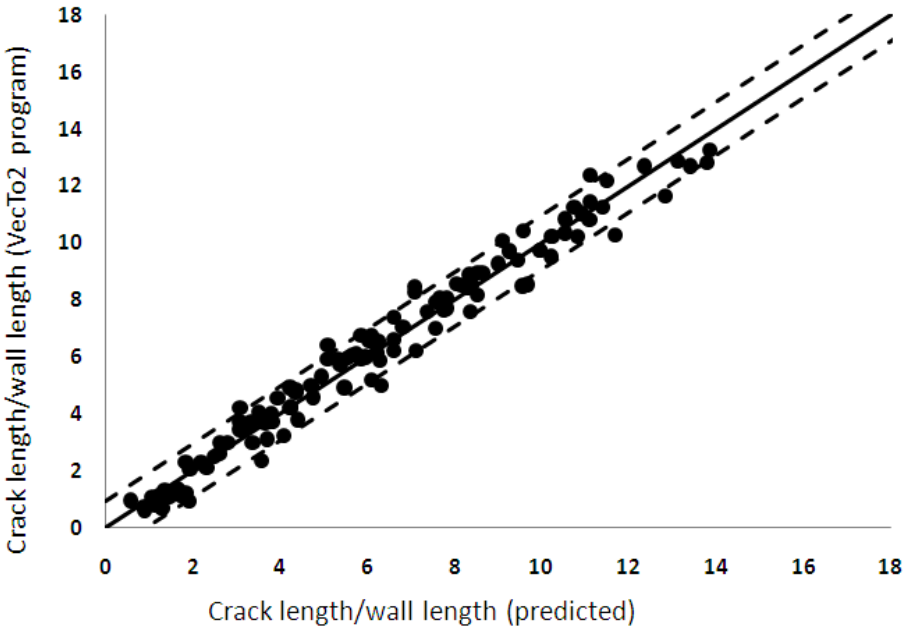

Table 5.5 Parameter statistics of updated model

Coefficients	Mean	COV	Correlation coefficient			
			θ_1	θ_4	θ_5	θ_6
θ_1	7.10	0.016	1.00	-0.48	-0.03	-0.19
θ_4	-0.71	0.10	-0.48	1.00	-0.63	-0.20
θ_5	-0.34	0.11	-0.03	-0.63	1.00	-0.19
θ_6	1.18	0.14	-0.19	-0.20	-0.19	1.00
σ	0.58	0.07	-	-	-	-

5.3.2 Normality of errors

Upon removal of the outliers, the normality of errors is checked for by plotting the inverse cumulative probability distribution of the model residuals using normal distribution function. This is shown in Figure 5.6. The scale of ordinate is not linear being closer near the median for the 25th and 75th percentiles of the normal distribution. The scale stretches out systematically by moving away from the median. This is to identify the data points which lie beyond the quantiles. Generally, the errors are considered to be distributed normally if they accumulated along the 1:1 line. The assumption of normality of errors is reasonable herein considering the majority of errors being close to straight line.

Figure 5.6 Normality plot

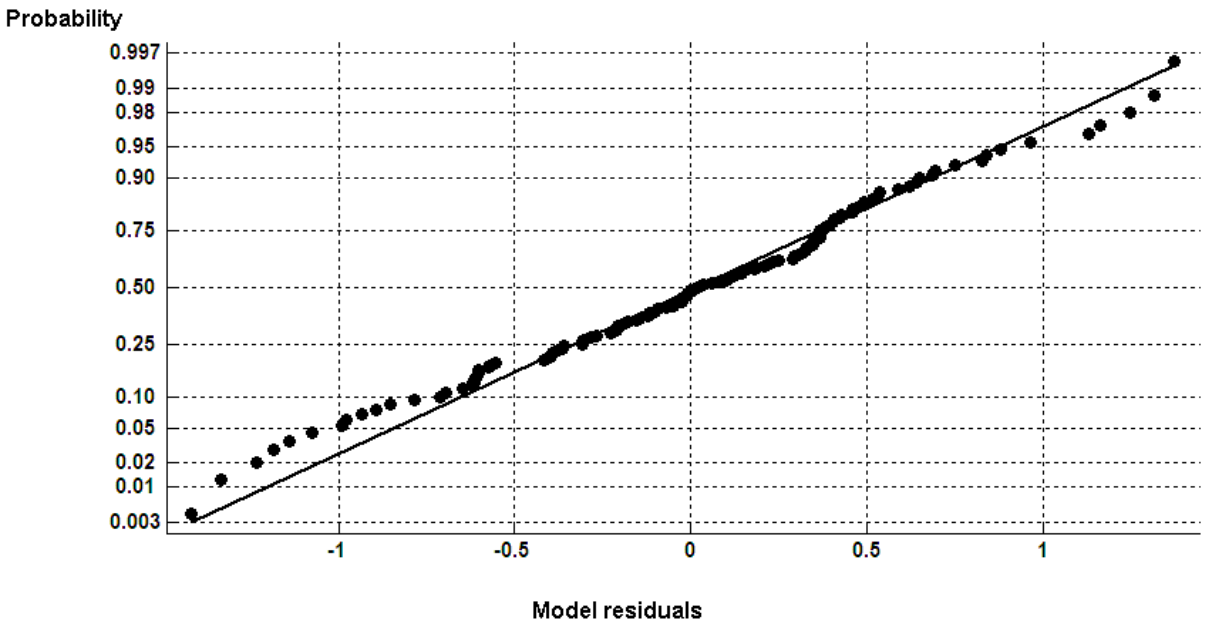

5.3.3 Heteroskedasticity

Heteroskedasticity refers to the condition where the model residuals depend on the variations in the values of independent variables. This is important because constancy of the model error (homoskedasticity) is one of the assumptions behind the theory of least square regression and hence probabilistic model development. In case this assumption is violated, model transformations can be used to remove heteroskedasticity. Chatterjee and Hadi (2006) provide a list of transformations for the variable y in order to stabilize the model variance. The transformations depend on the distribution of the y variables.

To check for possible heteroskedasticity, the squares of residuals of the model in Eq. (41) with updated parameters are plotted against the regressors. These plots are shown in the following pages. For all regressors, the squares of the residuals are found to lie within a band width which does not diverge as the values of regressors increase. This is an indication of homoskedasticity.

Figure 5.7 Plot of residuals against story drift

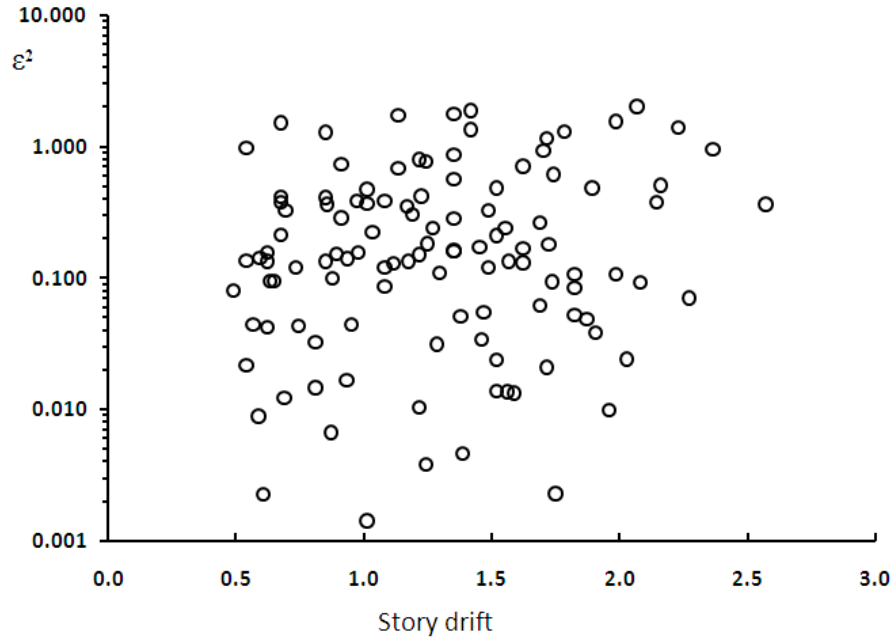

Figure 5.8 Plot of residuals against slenderness ratio

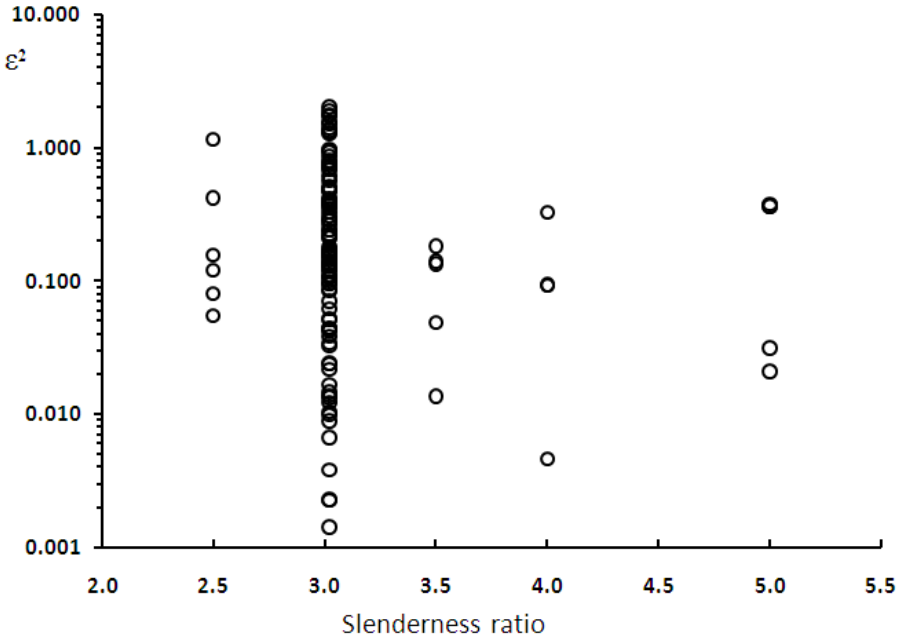

Figure 5.9 Plot of residuals against axial load ratio

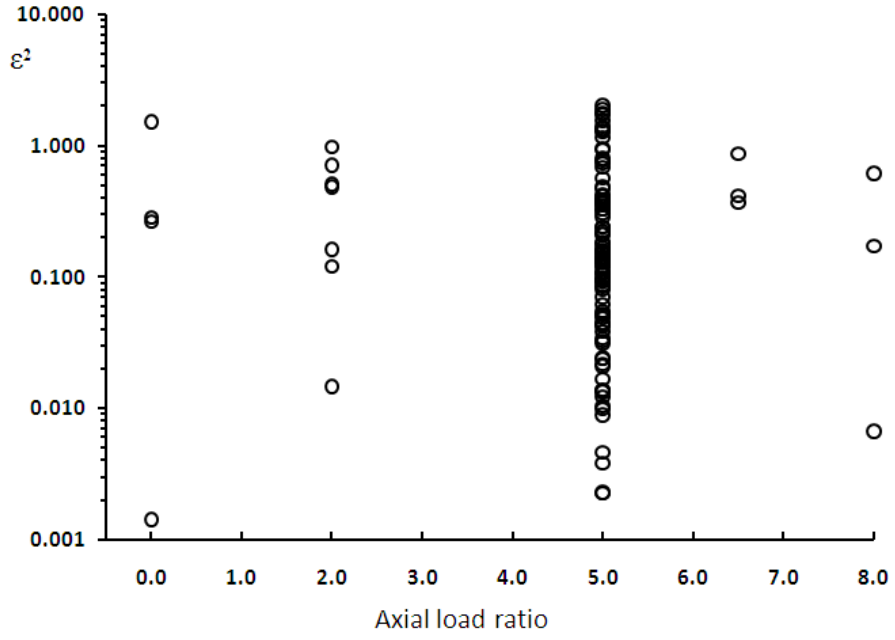

Figure 5.10 Plot of residuals against web flexural reinforcement ratio

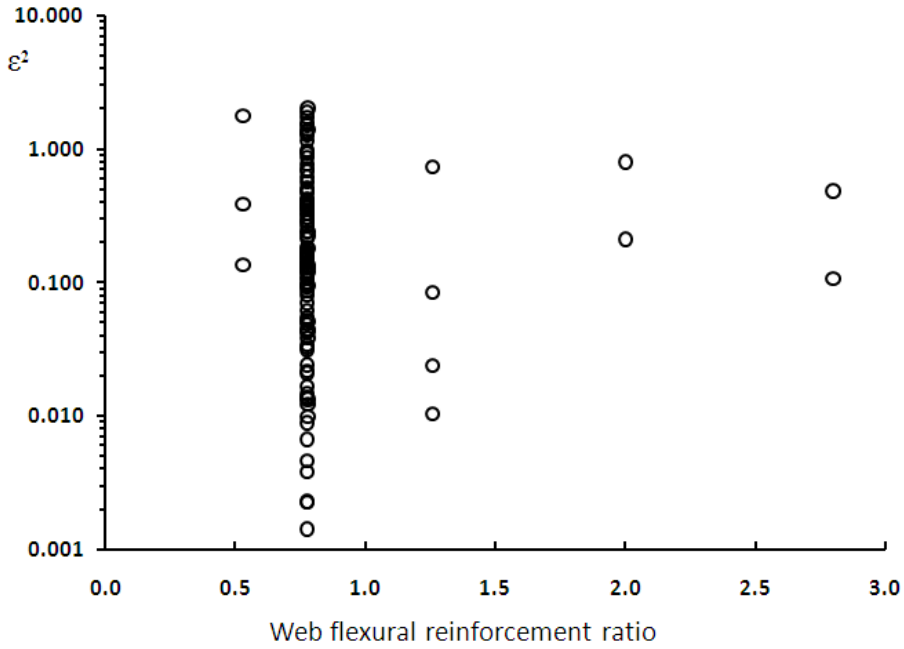

6 Conclusions and Recommendations

The probabilistic approach proposed herein puts forward a new methodology in the context of performance-based earthquake engineering. Through probabilistic model development, the approach estimates seismic losses to structures in terms of repair cost and time. Among the important outcomes of this approach are: a) incorporating all mathematical models, engineering parameters and information available for seismic damage prediction and loss estimation; b) accounting for all sources of uncertainty inherent in seismic loss analysis; c) facilitating the application of reliability analysis to develop various loss probability curves.

The proposed damage model to predict crack length in RC shear walls is an example of probabilistic model development procedure. Through this example, the explicit account of uncertainties is illustrated. In addition, insight on the effect of contributing design variables is achieved. The visual damage probabilistic models are considered as pioneering models in prediction of physical quantities of damage in the context of performance prediction. Nevertheless, the proposed model has limitations. First, analytical observations are used for model development. Certainly, this limits the model to analytical applications and the predicted results might not be as accurate as actual or experimental observations. Being based on a limited database of walls, the model is also only applicable on the range of design variables considered. It should be emphasized that the model is only for ductile walls with slenderness ratio between 2.5 to 5 with ductility ratio equal or great than 3. Clearly, model improvements can be achieved by further analysis of walls with additional parameters and broader range of design variables.

The context of this work can be extended in the future in several ways. First, the general probabilistic methodology proposed herein can be used to generate library of damage and loss models for various components in structures. In essence, the approach proposed herein is not limited to RC components but all types of structural components. The probabilistic model development procedure can also be applied to develop models of damage and loss for non-structural components which contribute the most in losses to a structure.

The proposed model of crack length can also be updated. This is achieved by inclusion of additional observations on cracking to walls. Clearly, laboratory test results are more representative of actual structural performance compared to analytical results. This leads to a plea for future laboratory testing in which intended measures of damage are recorded. Future work can also include development of repair cost and time probabilistic models for RC shear walls. Indeed, the ultimate application of the proposed methodology is for final loss estimations. The results of the proposed model in terms of the extent of cracking can be used in such models to determine the associated loss.

References

Adebar, P., Ibrahim, A. M. M., and Bryson, M. (2007). "Test of high-rise core wall: Effective stiffness for seismic analysis." *ACI Struct.J.,* 104(5), 549-559.

Adebar, P., and Van Leeuwen, J. (1999). "Side-face reinforcement for flexural and diagonal cracking in large concrete beams." *ACI Struct.J.,* 96(5), 693-704.

ATC 13. (1985). *Earthquake damage evaluation data for California.* Prepared by Applied Technology Council, funded by Federal Emergency Management Agency, Redwood City, CA.

ATC 24. (1992). *Guidelines for cyclic seismic testing of components of steel structures for buildings.* Prepared by Applied Technology Council, funded by Federal Emergency Management Agency, Redwood City, CA.

ATC 58. (2009). *Guidelines for seismic performance assessment of buildings.* Prepared by Applied Technology Council, prepared for Federal Emergency Management Agency, Redwood City, CA.

Banon, H., Biggs, J. M., and Irvine, H. M. (1981). "Seismic damage in reinforced concrete frames." *Journal of Structural Engineering,* 107(9), 1713-1729.

Berry, M. P., and Eberhard, M. O. (2005). "Practical performance model for bar buckling." *J.Struct.Eng.,* 131(7), 1060-1070.

Bohl, A. (2009). "Comparison of performance based engineering approaches." PhD thesis, University of British Columbia, BC, Canada.

Box, G. E. P., and Tiao, G. C. (1992). *Bayesian inference in statistical analysis.* Wiley Classics Library, Wiley-Interscience, .

Bozorgnia, Y., and Bertero, V. V. (2004). *Earthquake engineering: from engineering seismology to performance-based engineering.* CRC Press, Boca Raton, FL.

Chatterjee, S., and Hadi, A. S. (2006). *Regression analysis by example.* John Wiley and Sons Inc., Hoboken, New Jersey.

Collins, M. P., and Mitchell, D. (1987). *Prestressed concrete basics.* Canadian Prestressed Concrete Institute, Ottawa, Canada.

Corley, W. G., Fiorato, A. E., and Oesterle, R. G. (1981). *Structural Walls.* American Concrete Institute, Publication SP-72, Detroit, Michigan.

Cornell, C., and Krawinkler, H. (2000). *Progress and challenges in seismic performance assessment.*

CSA Standard A23.1. (2009). *Concrete design handbook.* Cement Association of Canada, .

de Borst, R., Remmers, J. J. C., Needleman, A., and Abellan, M. (2004). "Discrete vs smeared crack models for concrete fracture: Bridging the gap." *Int.J.Numer.Anal.Methods Geomech.,* 28(7-8), 583-607.

FEMA 306. (1998). *Evaluation of earthquake damaged concrete and masonry wall buildings.* Prepared for the Partnership for Response and Recovery, funded by Federal Emergency Management Agency, Washington, D.C.

FEMA 307. (1998). *Evaluation of earthquake damaged concrete and masonry wall buildings.* Prepared by the Applied Technology Council, prepared for the Partnership for Response and Recovery, Redwood City, CA.

FEMA 308. (1998). *Repair of earthquake damaged concrete and masonry wall buildings.* Prepared for the Partnership for Response and Recovery, funded by Federal Emergency Management Agency, Washington D.C.

FEMA 356. (2000). *Prestandard and complementary for the seismic rehabilitation of buildings.* Prepared by the American Society of Civil Engineers, prepared for the Federal Emergency Management Agency, Washington, D.C.

FEMA 445. (2006). *Next-generation performance-based seismic design guidelines.* Prepared for the Federal Emergency Management Agency, prepared by Applied Technology Council, Washington, D.C.

FEMA 461. (2007). *Interim testing protocols for determining the seismic performance characteristics of structural and nonstructural components.* Prepared by Applied Technology Council, prepared for Federal Emergency Management Agency, Washington, DC.

Gardoni, P. (2002a). "Probabilistic models and fragility estimates for structural components and systems." PhD thesis, University of California, Berkeley, CA.

Gardoni, P., Der Kiureghian, A., and Mosalam, K. M. (2002b). "Probabilistic capacity models and fragility estimates for reinforced concrete columns based on experimental observations." *J.Eng.Mech.,* 128(10), 1024-1038.

Haukaas, T., and Bohl, A. (2009). "Comparison of approaches for performance-based earthquake engineering." *Workshop on Performance-based Engineering, .*

Haukaas, T. (2008). "Unified reliability and design optimization for earthquake engineering." *Prob.Eng.Mech.,* 23(4), 471-481.

Haukaas, T., Talachian, S., and Elwood, K. J. (2010). "Probabilistic models for visual damage." *Advances in performance-based earthquake engineering,* Springer Dordrecht Heidelberg, London New York, 245-254.

Hidalgo, P. A., Ledezma, C. A., and Jordan, R. M. (2002). "Seismic behavior of squat reinforced concrete shear walls." *Earthquake Spectra,* 18(2), 287-308.

Igarashi, S., Cho, B. M., and and Maeda, M. (2009). "Development of analytical model for repairability evaluation of ductile columns." *Proceedings of the Japan Concrete Institute,* 901-906.

Jeffreys, H. (1961). *Theory of probability*. Clarendon, Oxford, U.K.

John, G. H. (1995). "Robust decision trees: removing outliers from databases." *Proceeding of the First International Conference on Knowledge Discovery and Data Mining,* AAAL Press, Menlo Park, CA, 174-179.

Kupfer, H. B., and Gerstle, K. H. (1973). "Behavior of concrete under biaxial stresses." 99 853-866.

Lang, K. (2002). "Seismic vulnerability of existing buildings." PhD thesis, Swiss Federal Institute of Technology, Zurich, Switzerland.

Lefas, I. D., Kotsovos, M. D., and Ambraseys, N. N. (1990). "Behavior of reinforced concrete structural walls. Strength, deformation characteristics, and failure mechanism." *ACI Struct.J.,* 87(1), 23-31.

Maekawa, K., Pimanmas, A., and Okamura, H. (2003). *Nonlinear mechanics of reinforced concrete.* Spon Press, New York.

MathWorks, I. (2009a). "Matlab." 7.8.0.

Oesterle, R. G., Aristizabal-Ochoa, J., Shiu, K. N., and Corley, W. G. (1984). "Web crushing of reinforced concrete structural walls." *Journal of the American Concrete Institute,* 81(3), 231-241.

Okamura, H., and Maekawa, K. (1991). *Nonlinear analysis and constitutive models of reinforced concrete*
. Giho-do Press, University of Tokyo.

Oluokun, F. A. (1991). "Prediction of concrete tensile strength from its compressive strength. Evaluation of existing relations for normal weight concrete." *ACI Mater.J.,* 88(3), 302-309.

Pagni, C. A., and Lowes, L. N. (2006). "Fragility functions for older reinforced concrete beam-column joints." *Earthquake Spectra,* 22(1), 215-238.

Palermo, D., and Vecchio, F. J. (2002). "Behavior and analysis of reinforced concrete walls subjected to reversed cyclic loading." *Rep. No. ISBN 0-7727-7553-2,* Department of Civil Engineering, University of Toronto, Toronto.

Palermo, D., and Vecchio, F. J. (2007). "Simulation of cyclically loaded concrete structures based on the finite-element method." *J.Struct.Eng.,* 133(5), 728-738.

Park, R., Priestley, M. J. N., and Gill, W. D. (1982). "Ductility of square-confined concrete columns." 108 929-950.

Park, Y., Ang, A. H. -., and Wen, Y. K. (1985). "Seismic damage analysis of reinforced concrete buildings." *J.Struct.Eng.,* 111(4), 740-757.

Paulay, P., and Priestley, M. N. J. (1992). *Seismic design of reinforced concrete and masonry buildings.* Wiley-Interscience, New York.

Petryna, Y. S., and Krätzig, W. B. (2005). "Compliance-based structural damage measure and its sensitivity to uncertainties." *Comput.Struct.,* 83(14), 1113-1133.

Popovics, S. (1973). "Numerical approach to the complete stress-strain curve of concrete." *Cem.Concr.Res.,* 3(5), 583-599.

Porter, K. A. (2003). "An overview of PEER's performance-based earthquake engineering methodology." *Proceedings, Ninth International Conference on Applications of Statistics and Probability in Civil Engineering (ICASP9),* Civil Engineering Risk and Reliability Association (CERRA), 973-980.

Ramamoorthy, S. K., Gardoni, P., and Bracci, J. M. (2006). "Probabilistic demand models and fragility curves for reinforced concrete frames." *J.Struct.Eng.,* 132(10), 1563-1572.

Rao, C. R., and Toutenburg, H. (1999). *Linear models: Least squares and alternatives.* Springer-Verlag New York Inc., New York, US.

Rosner, B. (1983). "Percentage points for a generalized ESD many-outlier procedure." *Technometrics,* 25(2), 165-172.

Rots, J. G. (1991). "Smeared and discrete representations of localized fracture." *Int.J.Fract.,* 51(1), 45-59.

Seckin, M. (1981). "Hysteretic behaviour of cast-in-place exterior beam-column-slab subassemblies." PhD thesis, Department of Civil Engineering, University of Toronto.

Takemura, H., and Kawashima, K. (1997). "Effect of loading hysteresis on ductility capacity of reinforced concrete bridge piers." *Journal of Structural Engineering (Japan),* 43A 849-585.

Thomsen IV, J. H., and Wallace, J. W. (2004). "Displacement-based design of slender reinforced concrete structural walls - Experimental verification." *J.Struct.Eng.,* 130(4), 618-630.

Thomsen IV, J. H., and Wallace, J. W. (1995). "Displacement-based design of reinforced concrete structural walls: Experimental studies of walls with rectangular and T-shaped cross sections." *Rep. No. CU/CEE-95/06,* Department of Civil and Environmental Engineering, Clarkson University, Potsdam, N.Y.

Tirasit, P., Kawashima, K., and Watanabe, G. (2005). "An experimental study on the performance of RC columns subjected to cyclic flexural-torsional loading." *Proceedings of 2nd International Conference on Urban Earthquake Engineering,* 357-364.

Vecchio, F. J. (2000). "Disturbed stress field model for reinforced concrete: Formulation." *Journal of Structural Engineering New York, N.Y.,* 126(9), 1070-1077.

Vecchio, F. J. (1999). "Towards cyclic load modeling of reinforced concrete." *ACI Struct.J.,* 96(2), 193-202.

Vecchio, F. J. (1992). "Finite element modeling of concrete expansion and confinement." *Journal of Structural Engineering New York, N.Y.,* 118(9), 2390-2406.

Vecchio, F. J., and Collins, M. P. (1993). "Compression response of cracked reinforced concrete." *Journal of Structural Engineering New York, N.Y.,* 119(12), 3590-3610.

Vecchio, F. J., and Collins, M. P. (1986). "Modified compression-filed theory for reinforced concrete elements subjected to shear." *Journal of the American Concrete Institute,* 83(2), 219-231.

Williams, M. S., and Sexsmith, R. G. (1995). "Seismic damage indices for reinforced concrete structures: A state-of-the-art review." *Earthquake Spectra,* 11(2), 319-349.

Wong, P. S., and Vecchio, F. J. (2002). *Vector2 & Formwork user's manual.* Department of Civil Engineering, University of Toronto.

Yang, T. Y., Moehle, J., Stojadinovic, B., and Der Kiureghian, A. (2009). "Seismic performance evaluation of facilities: Methodology and implementation." *J.Struct.Eng.,* 135(10), 1146-1154.

Zhang, Y., and Wang, Z. (2000). "Seismic behavior of reinforced concrete shear walls subjected to high axial loading." *ACI Struct.J.,* 97(5), 739-750.

Zhu, L., Elwood, K. J., and Haukaas, T. (2007). "Classification and seismic safety evaluation of existing reinforced concrete columns." *J.Struct.Eng.,* 133(9), 1316-1330.

Appendix A: Questionnaire

(Example Form with fictitious answers)

Type of Component: Reinforced concrete shear walls

Damage scenario	Repair action	Total repair cost	Repair time
Cracks of width less than 0.5mm	*No repair needed*	*N/A*	*N/A*
Cracks of width 0.5mm to 10mm	*Epoxy injection*	*$10 per foot of crack length*	*Approximately 4 columns per hour*
Cracks thicker than 10mm and spalling of cover concrete	*Remove cover and area-patch concrete*	*$500 per column*	*5 hours per column*
Buckling of reinforcing bars	*Cutting and splicing of bars, patching of concrete*	*$1,000 per column*	*One day per column*
Core crushing and severe buckling of bars	*Not repairable. Replace column or demolish building*	*N/A*	*N/A*

1) What are the assumptions behind the answers, and how uncertain are your estimates?

   The repair cost & times are rough assessments based on a two-person crew. In the aftermath of an earthquake, the cost is likely 20-30% higher, and the repair time will depend upon crew availability.

   Indirect costs (transportation, equipment, overhead) are included in the cost estimates.

2) Is additional cost involved for any test required before or after the application of epoxy injection?

Yes ☐ No ☐

If yes, please specify the amount: ----------

3) Is additional cost involved for any non-architectural coating as part of the epoxy injection?

Yes ☐ No ☐

If yes, please specify the amount: ----------

4) Are indirect costs of mobilization, etc included in your cost estimates above?

Yes ☐ No ☐

If not, can this indirect cost be taken as a percentage of the direct costs? Yes ☐ No ☐

If so, which percentage value? ----------

5) How much do rate the post-earthquake inflation (in the weeks/months after an earthquake)?

----

6) How much do you reduce the total cost due to economy-of-scale? ----------

7) Do you have general comments or suggestions for this research project?

Appendix B: Selection of Loading History

Two major factors should be considered while defining a target loading history. These include the identification of the target damage states and the associated demand control parameter (FEMA 461 2007). The selected damage state herein is the occurrance of repairable cracks in RC shear walls. This is mainly attributed to the response of walls after yielding of flexural reinforcement. It is well-known that prior yielding, the response of walls is mainly controlled by variations in the level of applied shear force while wall displacement is the major controlling parameter during post-yielding response. Considering the focus of this work on early damage to walls up to peak strength of response, the target loading history includes both force and displacement control parameters. Yielding is defined as the onset at which the control parameter changes from force- to displacement-based. To construct such loading history, two steps are followed herein. In the first step, a force-based loading history is selected up to yielding of walls. Next, some of the common loading histories used in the literature are evaluated to select a suitable displacement history for post-yielding response. All analyses are conducted in VecTor2 program.

Force-controlled loading

Force demands significantly depend on the type of components considered. Hence, no general force-based loading protocol exists (FEMA 461 2007). In this study, the force at which yielding of flexural reinforcement occurs, F_y, is considered as the maximum force up to which force-based loading is applied. The increments of loading are selected as 0.25%, 50% and 75% of F_y. Figure B.1 shows this loading history. A preliminary study is performed on the walls herein with

this loading history with application of one cycle per load level. It is observed that no repairable cracks with widths exceeding 0.5mm occur prior yielding. As understood earlier, this limit is set as the threshold beyond which repair is required. Occurrance of no repairable cracks prior yielding is expected considering the effect of axial load and the amount of flexural reinforcement provided in the walls considered. This leads to the conclusion that increasing the number of cycles would have no considerable effect on damage considering the elastic response of the walls. Hence, the same loading history with one cycle per amplitude level is satisfactory.

Figure B.1 Force-based loading history

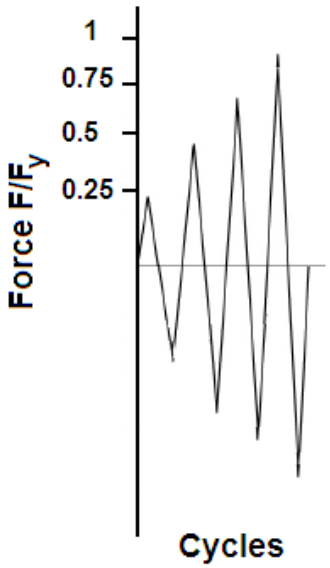

Displacement-based loading

Displacement-based loading history in this section is based on evaluating several loading protocols used in the literature. The loading histories considered are from FEMA 461 (2007), ATC 24 (1992) mainly for steel components and the works conducted by Takemura and Kawashima (1997) and Tirasit et al. (2005). The two histories used from the work by Takemura and Kawashima (1997) are numbered TP-2 and TP-3, similar to those used in the reference paper. Similarly, the one protocol used by Tirasit et al. (2005) is called TP95. These loading histories are shown in Figure B.2. The number of cycle repetitions and demand control parameters are also summarized in Table B.1. To evaluate the effect of displacement amplitude, the protocols TP-2 TP-3 are compared. In the former, amplitudes increase by half yield displacement whereas in the latter full yield displacement is used. To consider the effect of cycle repetitions on damage, ATC-24 and TP-2 are compared, having three and one repetitions per cycle, respectively. To also investigate the effect of displacement demand parameter FEMA 461, ATC-24 and TP95 are compared.

The protocol recommended by FEMA 461 (2007) is based on targeted maximum and minimum deformation amplitudes and predetermined number of increments, n. The increasing amplitudes are determined by the equation below in which a_1 and a_n are the minimum and maximum targeted displacements, respectively:

$$a_{i+1}/a_n = 1.4(a_i/a_n), \quad i=1,\ldots,n \qquad \text{Eq. (44)}$$

In this study, a_1 is considered as half the yield displacement and a_n is the displacement corresponding to peak strength of response equal to 136mm. Although usually values of n larger

than 10 are used, it is set to seven in here. Each cycle is repeated twice. This loading history is selected to evaluate the response of the wall while the effect of displacement at peak strength is taken into account at each demand level. To also evaluate the effect of a loading history based on story drift, the loading protocol TP95 used by Tirasit et al. (2005) is considered. In this loading history, the amplitudes increase based on increasing percentages of story drift. Three cycles are used for each amplitude level.

The remaining protocols are based on yield displacement. The protocol recommended in ATC 24 (1992) includes six elastic cycles followed by three repetitive cycles for each amplitude level after yielding. The factor of increase in amplitude after yield is equal to half of the yield displacement. It should be noted that the elastic cycles are not followed in this study as this range of response is evaluated by force-controlled loading histories. The protocol TP-2 used by Takemura and Kawashima (1997) has similar amplitude increments used in ATC-24 after yield but each cycle is repeated three times.

Table B.1 Details of protocols

Protocol	FEMA 461	ATC 24	TP2	TP3	TP95
Number cycle repetitions	2	3	1	1	3
Amplitude Control Parameter	Ratio of yield to displacement at peak load	Yield displacement	Yield displacement	Yield displacement	Global drift

Figure B.2 Loading history from literature

a) FEMA 461

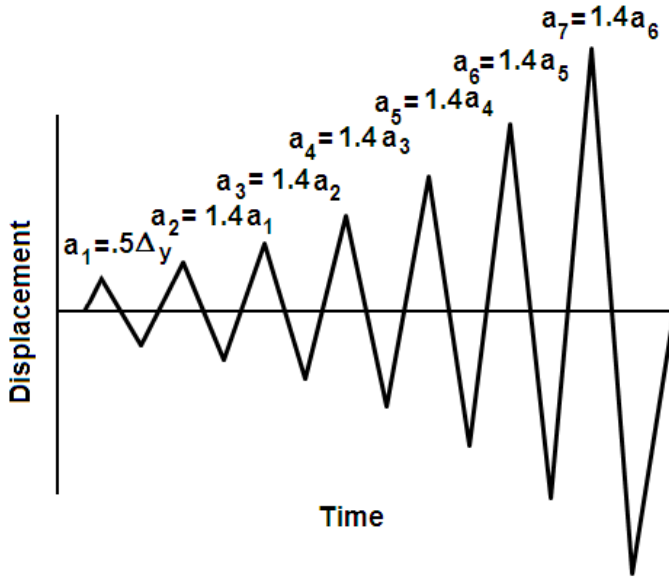

b) ATC-24

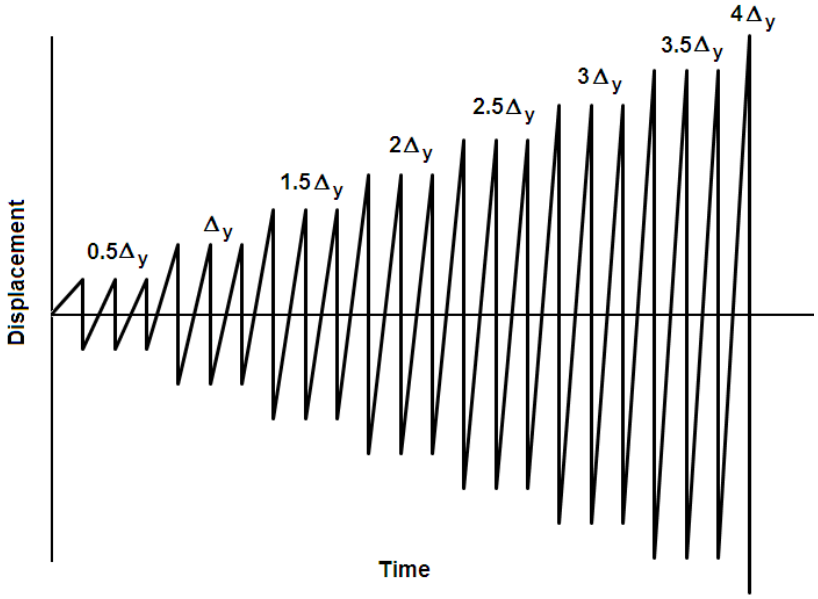

c) TP-2

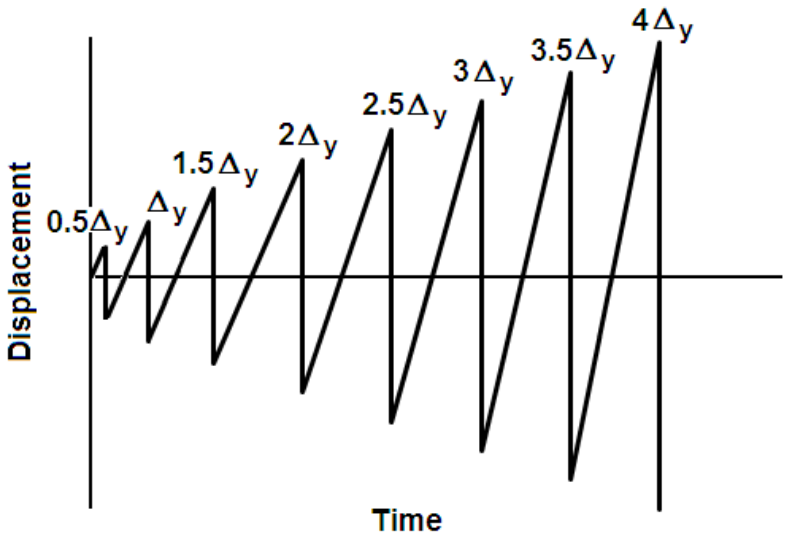
Displacement
0.5Δy
Δy
1.5Δy
2Δy
2.5Δy
3Δy
3.5Δy
4Δy
Time

d) TP-3

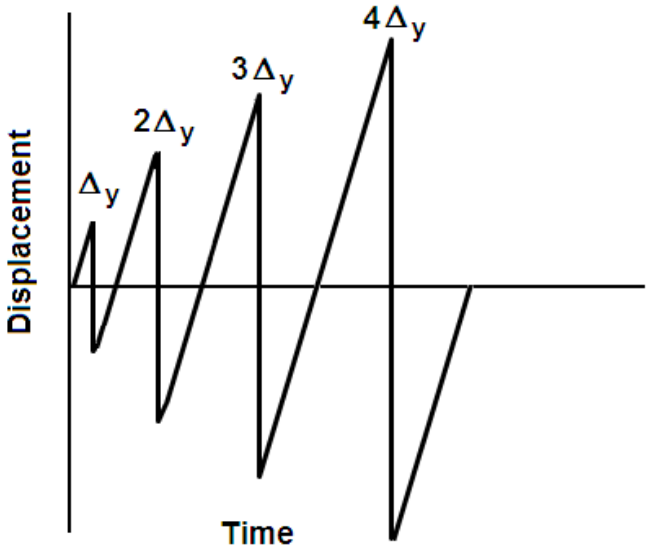
Displacement
Δy
2Δy
3Δy
4Δy
Time

e) TP-95

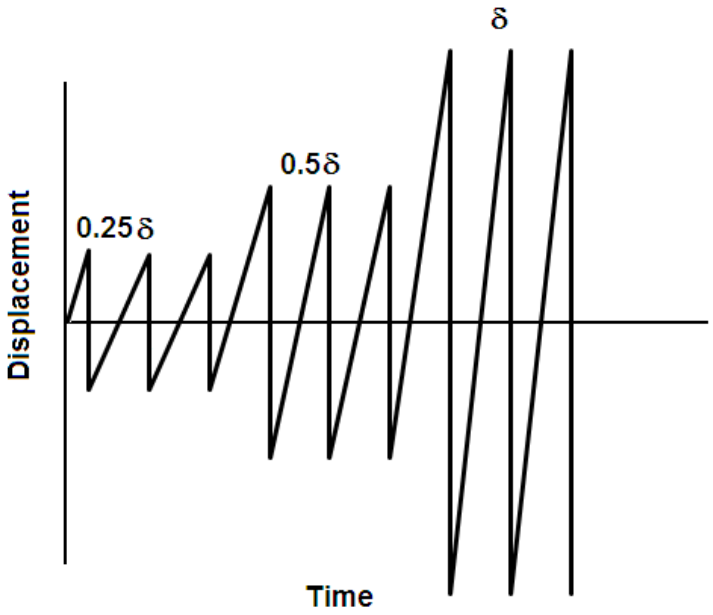

A typical RC shear wall is selected for this study. The properties of this wall are shown in Table B.2. This wall is selected due to having relatively low yield displacement of 35mm, facilitating the large number of reversed cyclic analyses performed. The wall has height-to-length ratio of 3 with length-to-width ratio of 9.8, similar to the majority of walls in the database. The backbone curve is obtained by pushing the wall monotonically up to its peak strength. This is because the analysis of post-peak response is not included for the study of the walls in the database.

Table B.2 Details of wall used for evaluation of loading protocols

Concrete Strength (MPa)	Ratio of flexural reinforcement		Ratio of horizontal reinforcement		Yield Strength of rebars	Axial load ratio
	Boundary	Web	Boundary	Web		
30	0.8%	0.88%	0.67%	0.67%	455MPa	2%

The comparison between the loading histories is as follows. The hysteresis responses from the above loading protocols are compared with the wall backbone response for obtained values of peak strength and their corresponding displacements. This is to identify the loading histories which lead to the least degradation of response. The hysteresis responses from each loading protocol compared with the backbone curve are shown in Figure B.3. The results are also summarized in Table B.3 as the ratios of peak strength and the corresponding displacement by each loading history to those obtained from the monotonic response.

Figure B.3 Comparison of backbone curve with loading protocols

a) FEMA 461

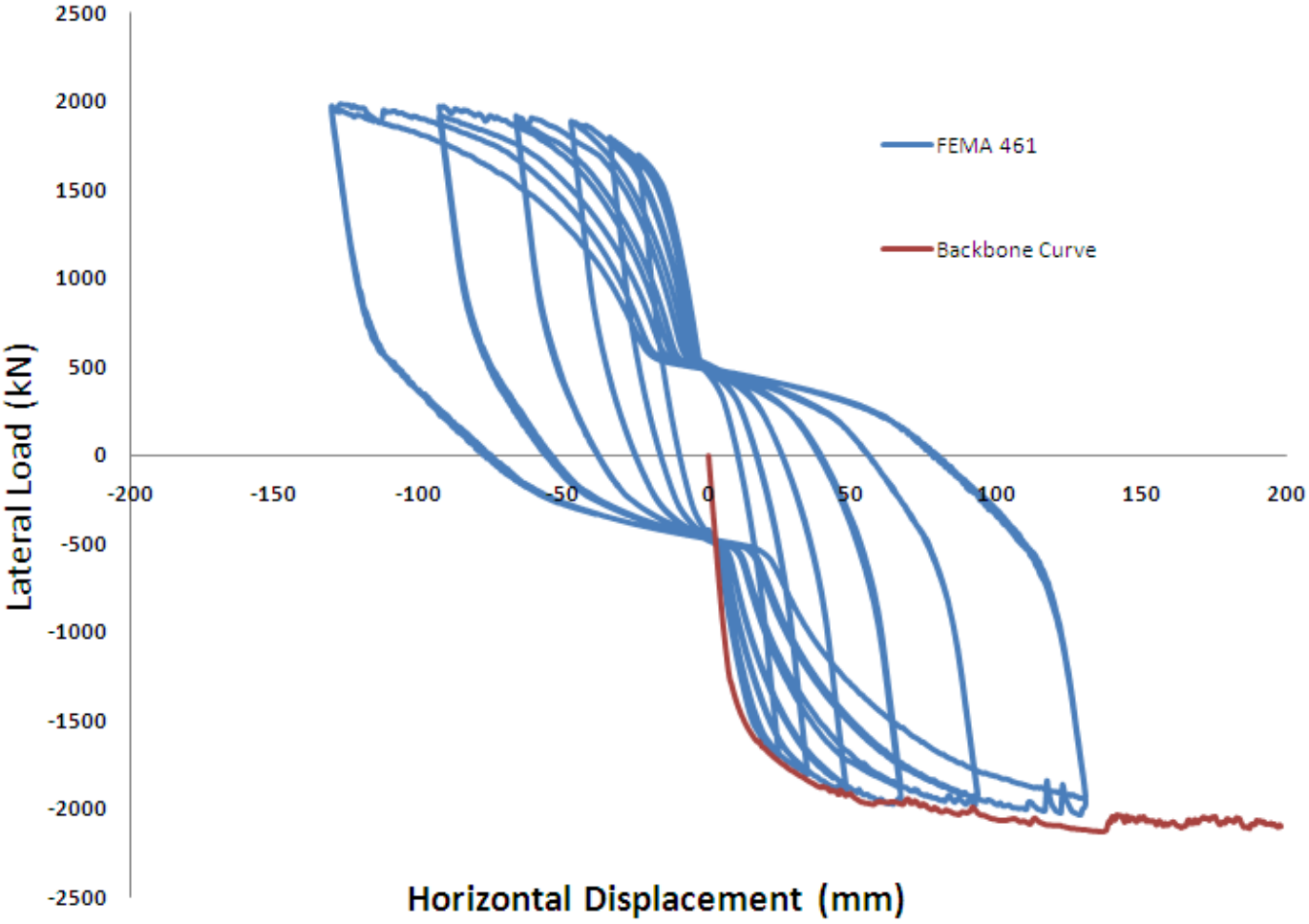

b) ATC-24

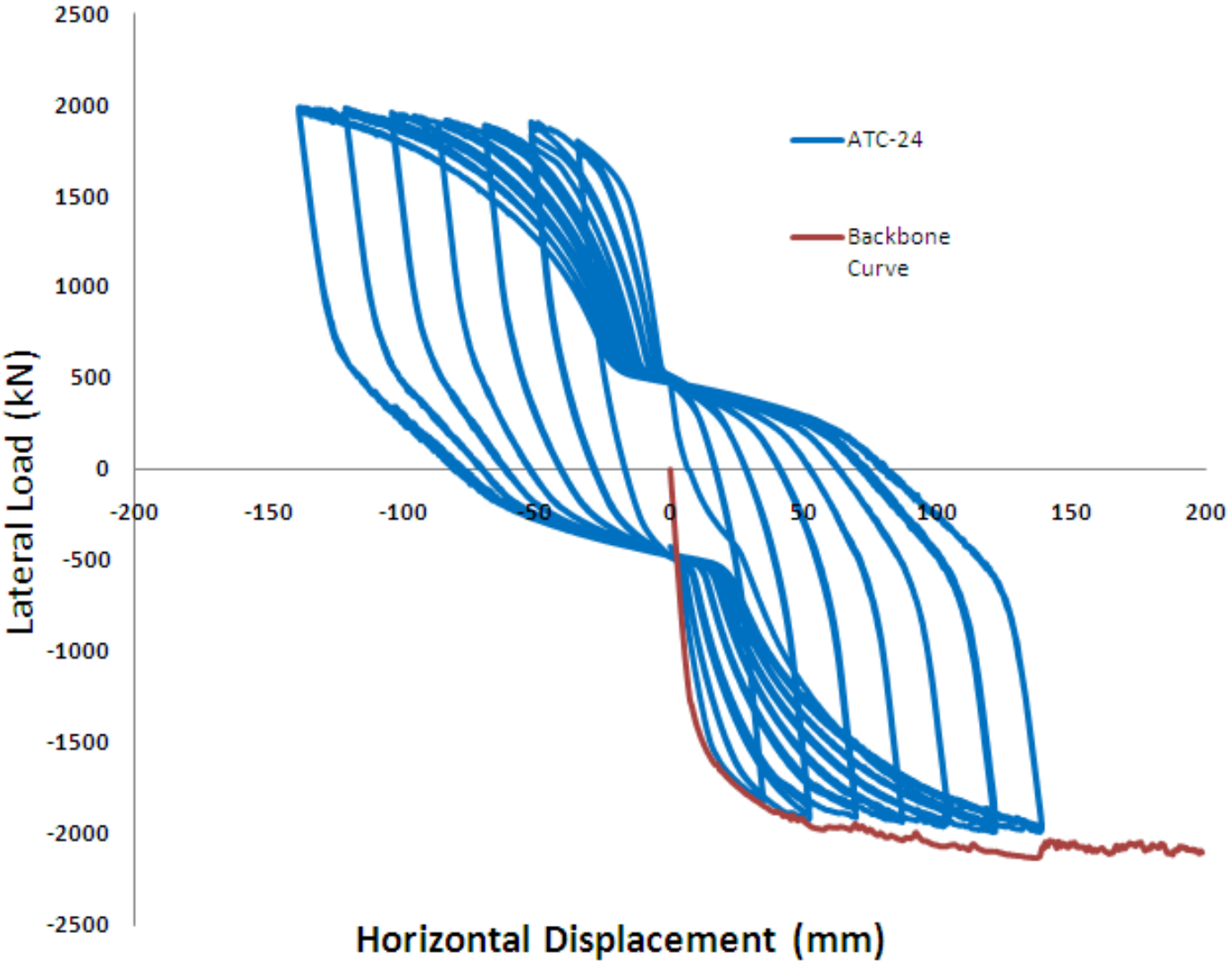
2500
2000
1500
1000
500
0
-500
-1000
-1500
-2000
-2500
-200
-150
-100
-50
0
50
100
150
200
Lateral Load (kN)
Horizontal Displacement (mm)
ATC-24
Backbone Curve

c) TP-2

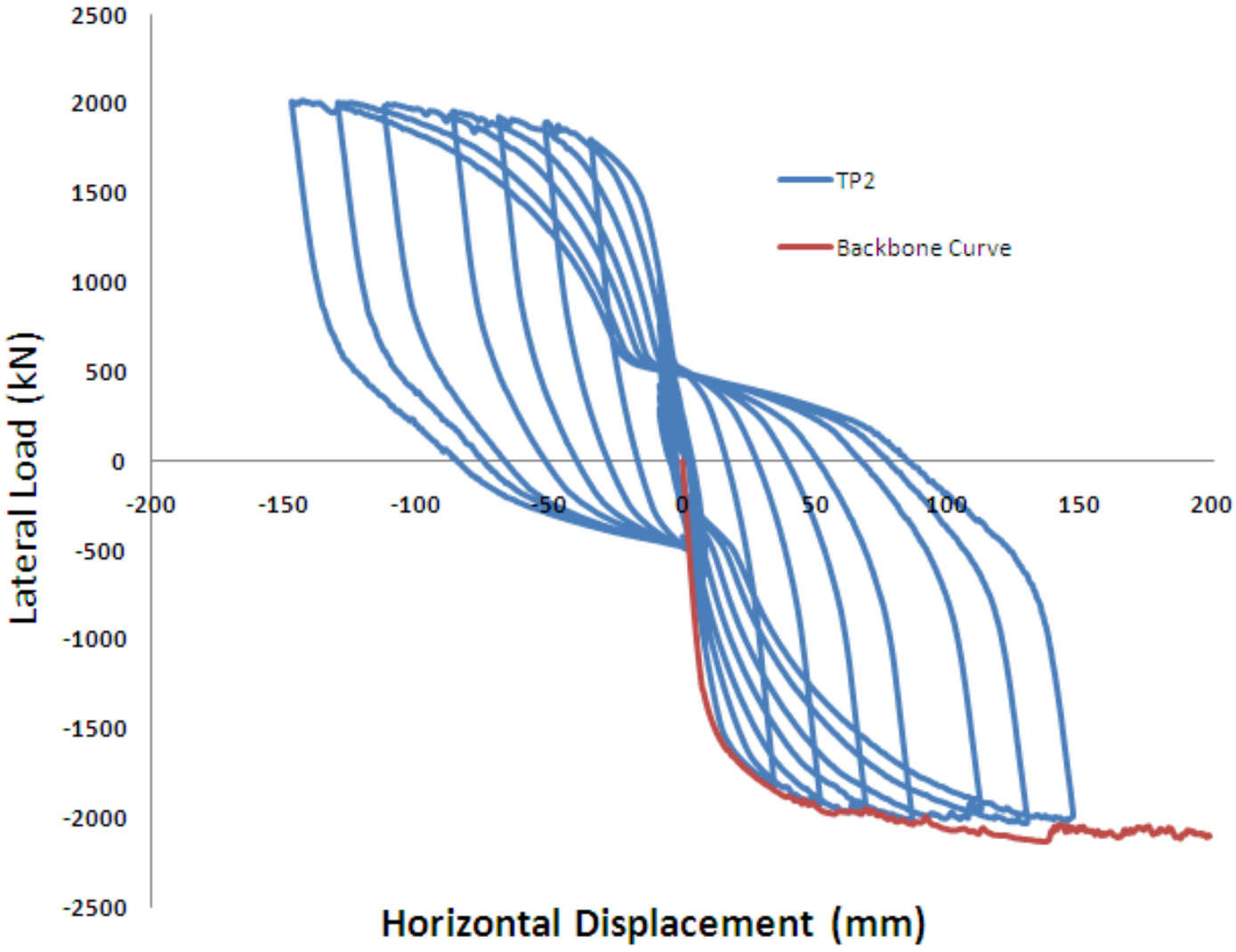
2500
2000
1500
1000
500
0
-500
-1000
-1500
-2000
-2500
-200
-150
-100
-50
0
50
100
150
200
Lateral Load (kN)
Horizontal Displacement (mm)
TP2
Backbone Curve

d) TP-3

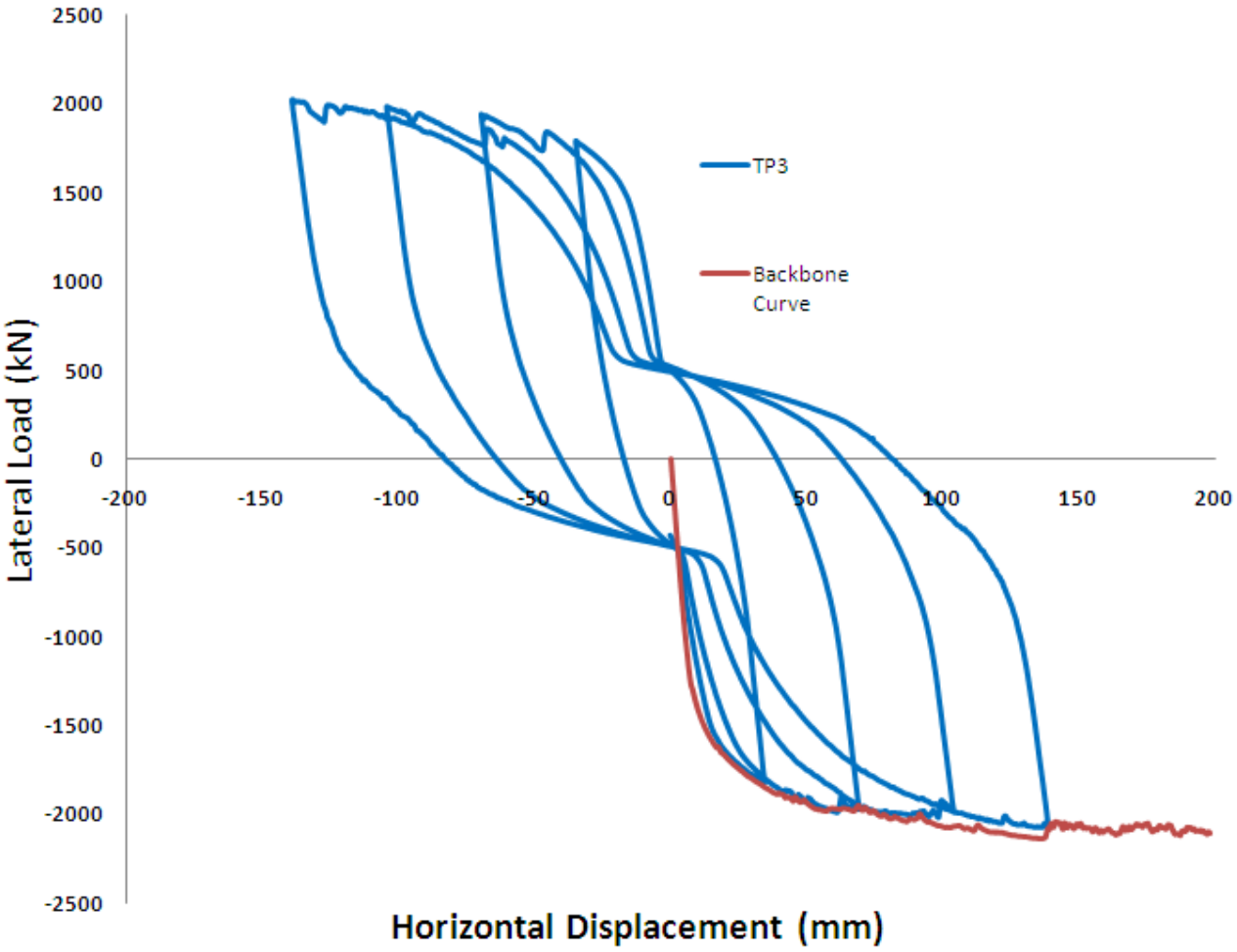
2500
2000
1500
1000
500
0
-500
-1000
-1500
-2000
-2500
-200
-150
-100
-50
0
50
100
150
200
Lateral Load (kN)
Horizontal Displacement (mm)
TP3
Backbone Curve

e) TP-95

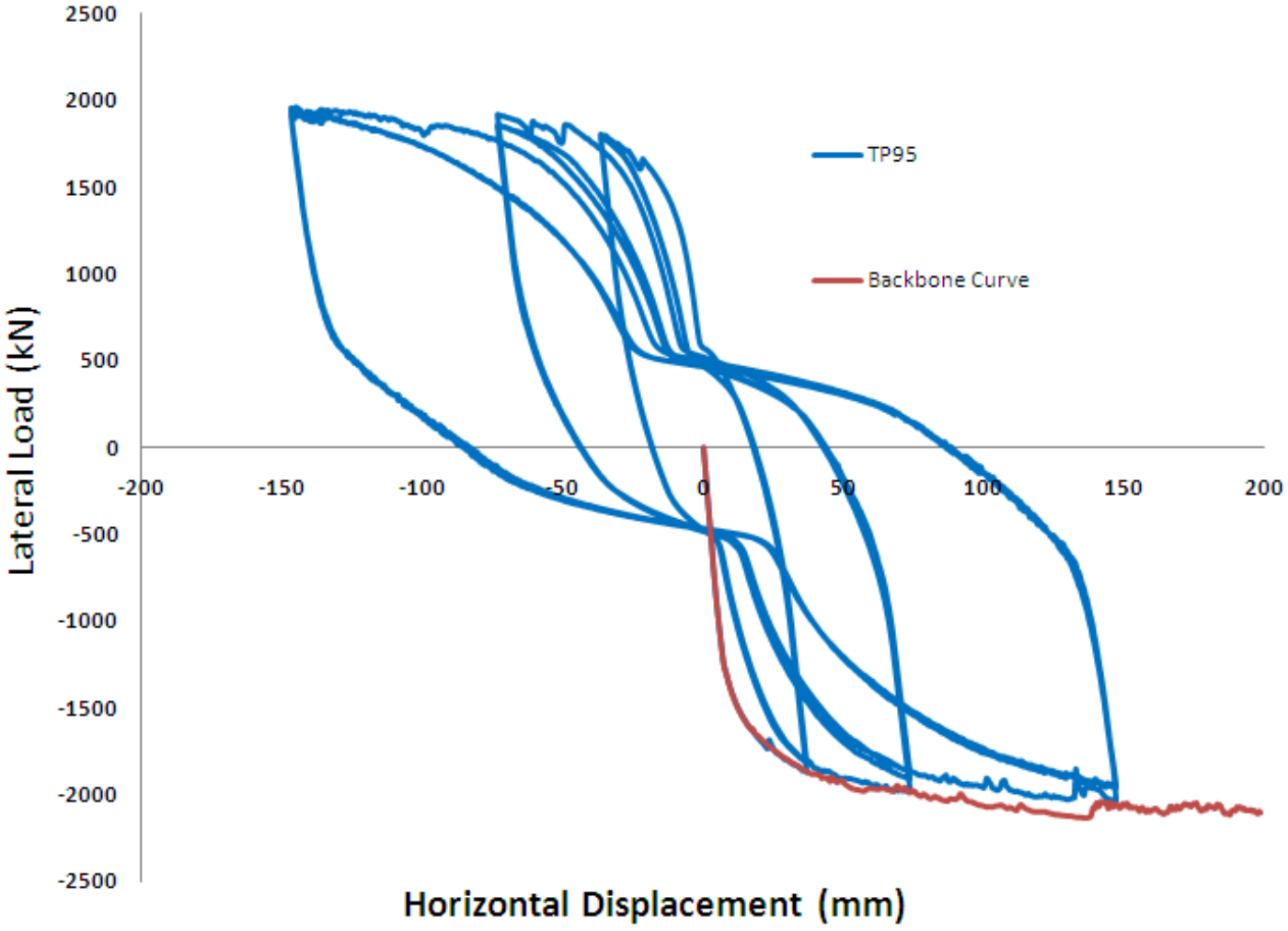
2500
2000
1500
1000
500
0
-500
-1000
-1500
-2000
-2500
-200
-150
-100
-50
0
50
100
150
200
Lateral Load (kN)
Horizontal Displacement (mm)
TP95
Backbone Curve

Table B.3 Comparison of loading protocols

Protocol	Maximum strength	Displacement corresponding to maximum strength	Relative absorbed energy
FEMA 461	95.5%	94.5%	1.01
ATC-24	93.2%	89%	1.51
TP-2	94.6%	1.05%	1.78
TP-3	97%	99.2%	1
TP-95	95.6%	1.07%	2.07

The maximum strengths achieved by all loading histories are fairly close to that of the monotonic response. Relative to other loading histories, TP-3 results in the highest ratio of maximum strength. Comparing the results of FEMA 461, ATC-24 and TP-95, it is found that the amplitude of displacement has no significant effect on the wall peak strength. Nevertheless, the large number of cycles associated with ATC-24 loading history results in lower ratio of obtained displacement. In other words, the relatively higher degradation as a result of numerous cycles forces the wall to reach its peak strength at earlier. The same conclusion can be also made for the repetition of the cycles at each amplitude level when comparing ATC-24 with TP-2. Observing close results obtained for the ratios of displacements- at maximum strength by hysteresis responses to that of the backbone curve- the selected loading history is TP-3 which results in relatively less degradation. TP-3 also includes one cycle repetition at each amplitude level which is advantageous when considering the large number of analyses required for the walls considered in the database.

The level of absorbed energy from each hysteresis response is compared to that of TP-3. Absorbed energy equal to the area under the load displacement curve is an indication of observed damage in the component. The large energy dissipations associated to ATC-24, TP-2 and TP-95 are due to the larger number of cycles involved.